PLOS COMPLEX SYSTEMS

RESEARCH ARTICLE

# The impact of excitability heterogeneity and synaptic coupling on resilience and stability of a macro-scale brain network

**Kalana G. Abeywardena**[1]*, **Jeremie Lefebvre**[2,3,4,5], **Taufik A. Valiante**[3,6], **Stark C. Draper**[1]

**1** Department of Electrical and Computer Engineering, University of Toronto, Toronto, Ontario, Canada, **2** Department of Biology, University of Ottawa, Ottawa, Ontario, Canada, **3** Krembil Brain Institute, University Health Network, Toronto, Ontario, Canada, **4** Department of Physics, University of Ottawa, Ottawa, Ontario, Canada, **5** Department of Mathematics, University of Toronto, Toronto, Ontario, Canada, **6** Institute of Medical Science; Institute of Biomedical Engineering; University of Toronto; Division of Neurosurgery, Department of Surgery; CRANIA (Center for Advancing Neurotechnological Innovation to Application); Max Planck-University of Toronto Center for Neural Science and Technology, Toronto, Ontario, Canada

* kalana.abeywardena@mail.utoronto.ca





**Citation:** Abeywardena KG, Lefebvre J, Valiante TA, Draper SC (2025) The impact of excitability heterogeneity and synaptic coupling on resilience and stability of a macro-scale brain network. PLOS Complex Syst 2(7): e0000057. https://doi.org/10.1371/journal.pcsy.0000057

**Editor:** Andre Fujita, University of Sao Paulo, BRAZIL

**Received:** September 12, 2024

**Accepted:** June 28, 2025

**Published:** July 28, 2025



**Data availability statement:** The neuroimaging-based brain connectivity data that support part of the findings of this study are publicly available from https://osf.io/befnx/. No other external data has been used in this study.

**Funding:** This work was supported by the Natural Sciences and Engineering Research Council (NSERC) of Canada through a Discovery Grant awarded to SCD (https://www.nserc-crsng.gc.ca/index_eng.asp).

## Abstract

Experimental, and computational studies have highlighted the abundance and significance of excitability and synaptic heterogeneity for network resilience, learning, and memory. However, these studies have been confined to cellular-level investigations, a spatial resolution that is inaccessible with clinical tools (i.e., electroencephalography, magnetoencephalography). Such clinical recordings capture local field potentials, representing brain activity at a coarser spatial scale than individual neurons. To understand how neuronal diversity affects large-scale activity, computational models and techniques are needed to examine the effects of heterogeneity on dynamics at these coarser scales. We therefore examine how intrinsic excitability heterogeneity in neuronal populations of the brain affects the stability and resilience of macro-scale brain networks against external stimulations. We use a macro-scale computational model where each node is a neural mass model with interacting excitatory and inhibitory sub-populations. Heterogeneities are represented using lumped parameters, and brain region dynamics are coupled through a global synaptic coupling parameter. Our numerical results show that excitability heterogeneity and synaptic coupling stabilize neural dynamics against external inputs, reducing amplitude variations and enhancing resilience at the macro-scale. Excitability heterogeneity also prevents the emergence of multiple equilibria. Although the global coupling parameter alone is less effective at reducing the emergence of multiple equilibria, it boosts the network's resilience when combined with heterogeneity. Thus, excitability heterogeneity stabilizes neural dynamics and simplifies the system's stable states on a broader spatial scale.

The funders had no role in study design, data collection and analysis, decision to publish, or preparation of the manuscript.

**Competing interests:** The authors have declared that no competing interests exist.

## Author summary

This study addresses a vital question: how does the diversity at the neuronal scale reflect at the larger spatial scale of brain dynamics? Most research has focused on patches within the brain when studying neuronal diversity, which is difficult to measure in a clinical environment that captures broader brain activity. Using computational techniques, the study highlights the cell-to-cell diversity among neurons in interconnected brain regions, stabilizes brain activity, and improves the network's resistance to external disruptions. Higher neuronal diversity in each brain region prevents the spread of undesired neural activities, such as seizures, across the brain. This knowledge effectively bridges the finer-scale biophysical diversity with its impact on coarser-scale dynamics.

## 1. Introduction

"Within cell-type heterogeneity" refers to individual differences between cells of the same type [1–3]. Although initially considered insignificant relative to between-cell-type heterogeneity, within-cell-type heterogeneity is now acknowledged as a fundamental organizing feature of the brain [4–6]. Computational studies have demonstrated that within-cell-type heterogeneity enhances information coding [7–13], stabilizes networks against the synchronous activity associated with seizures [14,15], and increases the resilience of neuronal networks to various factors that could potentially cause instabilities in dynamics [16,17]. Additionally, heterogeneous neural populations display enhanced learning and development of associative memory [12].

Such computational studies exploring neural heterogeneity have focused on modeling abstract "patches" of cortex representing either a single ensemble of neurons or a particular cortical layer within a brain region [13–15,18–23]. While studies at the cellular level highlight the significance of heterogeneity (see above), they face limitations in clinical translation since there is a mismatch between the scales of investigation. These limitations arise because clinical brain signals provide an "average" neuronal activity across brain regions [24,25]. Computational studies could expand cellular-level insights about neuronal heterogeneity to broader spatial scales that reflect diverse neuronal ensembles within anatomical brain regions.

Theories of population dynamics characterized by neural mass models often assume homogeneity within populations of spiking neurons [26–28]. This assumption allows for the abstraction of population activity using the dynamics of a single representative neuron [28]. However, it is recognized that variability in the electrophysiological and synaptic properties of neurons within a population can influence the parameters of the neural mass model's response function, particularly the slope, which may capture such diversity [26,29]. In fact, with the introduction of Brodmann areas [30], which represent regions of the cerebral cortex defined by cytoarchitecture, recent studies have explored inter-regional heterogeneity by modulating the macro-scale computational model parameters based on observed variability in specific properties across regions [27,31,32]. These studies have further deepened our understanding of inter-regional heterogeneity by integrating genetics, neurotransmitter distribution, and detailed anatomical data [32]. Gene expression profiles vary significantly across brain regions, indicating specialization based on unique genetic makeups [33–35]. The distribution of neurotransmitter receptors, such as glutamate (NMDA, AMPA) and $GABA_A$, $GABA_B$, also varies; distinct transcriptional profiles influence local circuitry and information processing [36]. Architectonic studies reveal variations in neuron

density, types, and connectivity patterns among regions, contributing to the brain's functional complexity [37]. Research correlating these structural differences with functional outcomes illustrates how anatomical features underpin cognitive and behavioral capabilities [29,37–41]. This perspective emphasizes the importance of regional heterogeneity in understanding brain function. It also highlights how disruptions in specific areas can lead to neurological and psychiatric disorders [35,36,41]. Therefore, recognizing regional neuronal heterogeneity is crucial to advance our understanding of brain dynamics and to develop targeted interventions for brain disorders.

## 1.1. Contribution

Regional heterogeneity is less frequently reflected biophysically in macro-scale computational models of the brain. Recent studies link this heterogeneity to variations in excitation-to-inhibition (E/I) neuron ratios across regions [29,36,37,41–43]. These properties define the parameters of the neural mass model at specific nodes, leading to heterogeneous temporal dynamics across the network. However, these studies assume that the excitatory and inhibitory sub-populations within a brain region share the same response function slope, modulated by a single E/I ratio. This simplification overlooks a key point from [26]: the slope of each population's response function should reflect the diversity of firing thresholds among its neurons. These studies focus on establishing the importance of diversity among brain regions, rather than analyzing how the diversity within each sub-population in a given brain region affects macro-scale dynamics in a network. By overlooking this heterogeneity, models may fail to capture the distinct contributions of excitatory and inhibitory populations to network dynamics. Additionally, the studies on regional heterogeneity do not explore how within-cell-type heterogeneity influences stability, resilience, or trivialization properties at the macro scale. Moreover, they do not address whether insights from neuronal-level studies on heterogeneity [13,14,20,44] align with, or differ from, those observed at the macro scale.

In contrast, this paper introduces a theoretical framework that defines the dynamics of structurally interconnected neural populations at a broader spatial scale, termed the *macro-scale*, while relaxing the assumption of local homogeneity within each anatomical region. This framework incorporates varying intrinsic excitability heterogeneity of neurons into the macro-scale dynamic modeling of each brain region. Drawing inspiration from [14], we focus on changes in neuronal firing thresholds as the key intrinsic excitability property. To this end, we consider an Amari-type neural mass model [45], which shares a similar linear stability formulation of the Wilson-Cowan model [26]. We parameterize the excitability heterogeneity of each sub-population in each node as the variance of firing thresholds within the neuronal ensemble. Our study investigates how excitability heterogeneity influences stability, resilience, and emergence of multi-stable states in macro-scale brain dynamics as external stimulation varies. This research highlights the dynamical consequences of intrinsic neuronal variability on macro-scale brain dynamics through interconnected brain regions, effectively bridging properties from the micro-level to the macro-level.

To investigate, we construct a generic macro-scale brain network with each node representing a brain region containing excitatory and inhibitory sub-populations. We use the neural mass model in [14] to define the dynamics at each node over a time scale spanning a few seconds. The dynamics of the nodes are linearly coupled between their excitatory sub-populations. The coupling efficacy is determined by structural connectivity measured via the white matter tracts between the regions [46], and a global synaptic coupling parameter. We apply a constant stimulation over the simulation time to a single node in the network

mimicking the modulatory, environmental, and stimuli-induced perturbations acting on a specific brain region on a slow time scale. Network stability is assessed using temporally averaged Lyapunov exponents. Equilibria of the neural dynamic field are computed numerically, and the system state is analyzed through linearization via the eigendecomposition of the Jacobian matrix at each equilibrium. Initially, numerical studies focus on a simple two-node macro-scale brain network, with subsequent investigations expanding the network size with empirical connectome data to assess the generalizability of our findings.

Our numerical investigations of a two-node macro-scale network demonstrate that both excitability heterogeneity and synaptic coupling are essential for stabilizing neural dynamics under external stimulation, with excitability heterogeneity having a more significant impact. Additionally, higher levels of excitability heterogeneity suppress the emergence of multiple equilibria (trivialization) within the neural dynamic field under a given stimulation. This heterogeneity within macro-scale populations also generates stable system states at the equilibria, even in the face of significantly higher external stimulation, indicating greater resilience. Although the global coupling parameter has a comparatively lesser impact on system trivialization than excitability heterogeneity, it nonetheless enhances resilience against external disturbances. Furthermore, our results highlight the nuanced influence of excitability heterogeneity on stability and trivialization, emphasizing its dependency on the specific sub-population in which it manifests. The findings from the two-node macro-scale brain network generalize well to a multi-node macro-scale network, representing a more complex and realistic network architecture of the brain.

### 1.2. Outline

Other than a brief discussion of notation (next), the rest of the paper is arranged as follows. In Sect 2, we introduce the computational model for a coupled macro-scale brain network, along with the metrics used to measure the system properties. In Sect 3, we present the numerical results on how the interplay between underlying neural excitability heterogeneity and the global coupling parameter influences the stability and trivialization of a brain network using a two-node macro-scale network. We extend the analysis to a multi-node network and present the results in Sect 4. In Sect 5, we offer a concise discussion outlining our main discoveries and the constraints of our analysis. Finally, we conclude our contribution in Sect 6.

### 1.3. Notation

We use $[N]$ to denote the index set $\{1, ..., N\}$ for any $N \in \mathbb{Z}_+$. For any $L \in \mathbb{Z}$, we use $[N] + L$ to denote shifted index set $\{1 + L, ..., N + L\}$. We use $\mathbb{I}_n$ to denote the identity matrix of size $n \times n$ and $\mathbf{1}_n$ to represent the all-ones vector of size $n$. We denote vectors and matrices using bold-faced lower and upper-case letters. We simplify the notation for $\mathbf{z}(t) = \left[z_n(t)\right]^T \in \mathbb{R}^N$, as $\mathbf{z} = \left[z_n\right]^T$ and define $\dot{\mathbf{z}} = \left[\dot{z}_n\right]^T \in \mathbb{R}^N$ with $\dot{z}_n = \frac{dz_n}{dt}$ denoting the temporal derivative of each element $n \in [N]$. Sets are denoted by calligraphic font e.g., $\mathcal{Z}$. The cardinality of a finite set $\mathcal{Z}$ is denoted by $|\mathcal{Z}|$. For $z = a + j\,b \in \mathbb{C}$, we define $|z| = \sqrt{a^2 + b^2}$ where $a = \Re\{z\}$ and $b = \Im\{z\}$.

## 2. Materials and methods

To analyze the effect of excitability heterogeneity and synaptic coupling, each macro-scale brain region is mathematically modeled as a node in a spatially distributed brain network. The dynamics of each node are defined using the neural mass model in [14], which is derived from the diffusion approximation [47] of a network of Poisson spiking neurons. The terms

*brain region* and *node* will be used interchangeably to refer to the macro-scale anatomical brain regions in the modeled brain network. Each node will have interacting excitatory (E) and inhibitory (I) neural sub-populations. For a single node, an Amari-type model restricted to a spatially uniform (homogeneous) kernel [14,45,48–50] defines the dynamics as:

$$\dot{\boldsymbol{u}} = \mathbf{T}\left(-\mathbf{u} + \mathbf{W}\overline{\mathbf{F}}(\mathbf{u},\boldsymbol{\sigma}) + \mathbf{i}_0 + \mathbf{i}_t\right), \tag{1}$$

where $\mathbf{u} = [u_{\mathrm{e}}, u_{\mathrm{i}}]^T \in \mathbb{R}^2$ is a stacked vector of the mean-field dynamics of E and I sub-populations. Similarly, $\boldsymbol{\sigma} = [\sigma_{\mathrm{e}}, \sigma_{\mathrm{i}}]^T \in \mathbb{R}^2$ is a stacked vector of the underlying excitability heterogeneity parameters of E and I sub-populations. The vector $\mathbf{i}_0 = [I_{\mathrm{e},0},\ I_{\mathrm{i},0}]^T \in \mathbb{R}^2$ represents the bias currents applied to each sub-population whereas $\mathbf{i}_t = [I_{\mathrm{e},t},\ I_{\mathrm{i},t}]^T \in \mathbb{R}^2$ represents the modulatory signals on each sub-population to perturb the system states. The matrix $\mathbf{T}$ represents the relative time-scaling of the sub-populations, i.e., $\tau_{\mathrm{e}}, \tau_{\mathrm{i}}$. The matrix $\mathbf{W}$ represents the intra-node connectivity matrix between E-I sub-populations using the intra-node synaptic weights $w_{\mathrm{ee}}, w_{\mathrm{ei}} > 0$ and $w_{\mathrm{ie}}, w_{\mathrm{ii}} < 0$. These two matrices are defined as

$$\mathbf{T} = \begin{bmatrix} \frac{1}{\tau_{\mathrm{e}}} & 0 \\ 0 & \frac{1}{\tau_{\mathrm{i}}} \end{bmatrix} \text{ and } \mathbf{W} = \begin{bmatrix} w_{\mathrm{ee}} & w_{\mathrm{ie}} \\ w_{\mathrm{ei}} & w_{\mathrm{ii}} \end{bmatrix}.$$

The vectorized mean-field non-linear function $\overline{\mathbf{F}}(\mathbf{x},\mathbf{s}) : \mathbb{R}^4 \to \mathbb{R}^2$ is described by $\overline{\mathbf{F}}(\mathbf{x},\mathbf{s}) = [F_\beta(x_1,s_1), F_\beta(x_2,s_2)]^T$ with $F_\beta(x,s)$ is defined as:

$$F_\beta(x,s) = \int_{-\infty}^{\infty} \frac{1}{1+\exp(-\beta(x+\theta))} \varphi(\theta;s)\, d\theta, \tag{2}$$

where $\beta$ is the non-linear gain of the activation function, and $\varphi(\theta;s) = \frac{1}{\sqrt{2\pi s^2}} e^{-\frac{\theta^2}{2s^2}}$ is a zero-mean Gaussian distribution whose variance $s^2 = (\sigma_{\mathrm{y}})^2$ for $\mathrm{y} \in \{e,i\}$ represents the dispersion of rheobases/firing thresholds of the neurons in E and I sub-populations of a node. Eq (2) explicitly defines the mean-field response of a neuronal ensemble based on its level of heterogeneity, aligning with the principles outlined in [26]. Specifically, excitability heterogeneity leads to a greater representation of both low-threshold and high-threshold neurons within the population as noted in prior studies [13,20]. Low-threshold neurons, which have higher firing rates, tend to pull $F_\beta(s,x)$ upward, while high-threshold neurons with lower firing rates tend to push it downward. This pull-push effect of diversely thresholded neurons extends the linear portion within the mean-field firing function. As heterogeneity increases (i.e., $\sigma \to \infty$), the average firing rate converges to 0.5, due to the balanced push-pull effect from the well-diverse neuron population. This behavior is illustrated in Fig 1 for a generic neuronal population.

Interactions among the macroscopic brain regions in the local brain network are introduced as the edges between the nodes in the network. We assumed linear coupling among E sub-populations of each node. The dynamics of node $n \in [N]$ in the macroscopic brain network can be described as

$$\dot{\boldsymbol{u}}^n = \mathbf{T}^n\Big(-\mathbf{u}^n + \mathbf{W}^n\overline{\mathbf{F}}(\mathbf{u}^n,\boldsymbol{\sigma}^n) + \mathbf{i}_0^n + \mathbf{i}_t^n + \mathbf{D}^{\mathbf{s}} K_{\mathrm{glob}} \sum_{m=1}^{N} p_{nm}\mathbf{u}^m\Big), \tag{3}$$

where $N$ is the number of brain regions in the network, $K_{\mathrm{glob}}$ is the global coupling parameter, and $\mathbf{D}^{\mathbf{s}} = \mathrm{diag}(1,0)$. We define $k_{nm} = K_{\mathrm{glob}} \cdot p_{nm}$ as the effective synaptic coupling between node $n$ and $m$ where $p_{nm} \in [0,1]\ \forall n,m \in [N]$ defines the weights of normalized structural

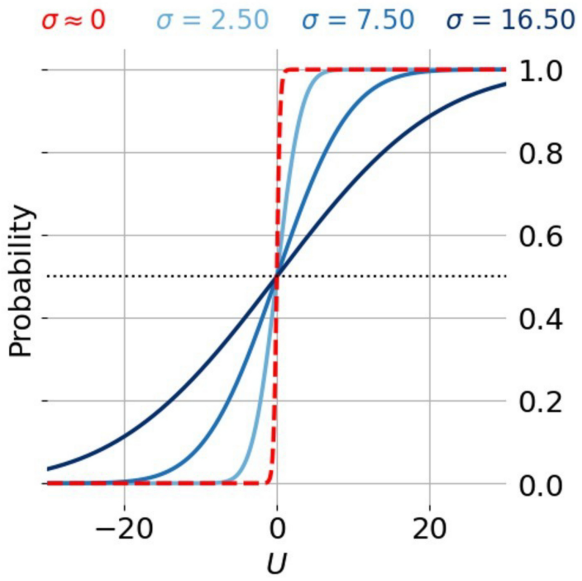


**Fig 1. Excitability heterogeneity changes the mean-field firing function.** For lower $\sigma$, the mean-field firing function is highly non-linear and similar to a single neuron firing characteristics. As $\sigma$ increases, the firing functions become more linear for a wide range of pre-synaptic neural activity.

https://doi.org/10.1371/journal.pcsy.0000057.g001

connectivity (association) between the two nodes. Following previous work on whole-brain modeling [27,29,51], $K_{\text{glob}}$ is a free controlling parameter that we vary systematically to study the dynamics of the network when its connectivity changes from weak to strong. We define the normalized structural connectome matrix as $\mathbf{P} = \left[p_{nm}\right] \in \mathbb{R}^{N\times N}$ that represents the associations between the network nodes. We statistically sample $\widetilde{\mathbf{P}} = \left[\tilde{p}_{nm}\right]$ using a standard exponential distribution in which each $\tilde{p}_{nm} \sim \text{Exp}(1)$ for $n, m \in [N]$ and $n \neq m$. The columns (and rows) of $\widetilde{\mathbf{P}}$ are arranged in such a way that the degree of connectivity of the nodes is in decreasing order. We obtain $\mathbf{P} = \left[p_{nm}\right]$ after normalizing $\widetilde{\mathbf{P}}$ so that the sum of connectivity weights for each node, i.e. the degree of the node, does not exceed 1 i.e., $\sum_{m=1}^{N} p_{nm} \leq 1 \; \forall n \in [N]$. In addition, $p_{nm} = p_{mn} \; \forall n, m \in [N]$, which suggests that the network is an undirected graph. In addition, there are no self-loops, i.e. $p_{nn} = 0$.

Following Eq (3), we derived the vectorized dynamics of the macro-scale brain network. Let $\mathbf{u}_{\text{net}} = \left[\mathbf{u}^n\right]^T \in \mathbb{R}^{2N\times 1}$ be the stacked vector of dynamics of each node. Let $\boldsymbol{\sigma}_{\text{net}} = \left[\boldsymbol{\sigma}^n\right]^T \in \mathbb{R}^{2N\times 1}$ be the stacked vector of heterogeneity parameters of each node. Let $\mathbf{W}_{\text{net}} = \text{diag}(\left[\mathbf{W}^n\right]) \in \mathbb{R}^{2N\times 2N}$ be the intra-node synaptic weight matrix for the network and let $\mathbf{T}_{\text{net}} = \text{diag}(\left[\mathbf{T}^n\right]) \in \mathbb{R}^{2N\times 2N}$ be the time constant matrix for the network. Further, define

$$\mathbf{D}_{\text{net}} = \begin{bmatrix} 1 & 0 & 0 & 0 & \dots & 0 & 0 & 0 & 0 \\ 0 & 0 & 1 & 0 & \dots & 0 & 0 & 0 & 0 \\ \vdots & & \vdots & & \ddots & & \vdots & & \vdots \\ 0 & 0 & 0 & 0 & \dots & 1 & 0 & 0 & 0 \\ 0 & 0 & 0 & 0 & \dots & 0 & 0 & 1 & 0 \end{bmatrix} \in \mathbb{R}^{N\times 2N}.$$

Using the above definitions, the network dynamics can be described as

$$\dot{\boldsymbol{u}}_{\text{net}} = \mathbf{T}_{\text{net}}\Big(-\mathbf{u}_{\text{net}} + \mathbf{W}_{\text{net}}\overline{\mathbf{F}}_{\text{net}}(\mathbf{u}_{\text{net}}, \boldsymbol{\sigma}_{\text{net}}) + (\mathbf{i}_0)_{\text{net}} + (\mathbf{i}_t)_{\text{net}} + K_{\text{glob}}\mathbf{P}_{\text{net}}\mathbf{u}_{\text{net}}\Big). \quad (4)$$

In the above, $\mathbf{P}_{\text{net}} = \mathbf{D}_{\text{net}}^T\mathbf{P}\mathbf{D}_{\text{net}} \in \mathbb{R}^{2N\times 2N}$ is an augmented connectivity matrix, which indicates that the nodes are connected through their E sub-populations. $(\mathbf{i}_0)_{\text{net}} = \left[\ \mathbf{i}_0^n\ \right]^T \in \mathbb{R}^{2N\times 1}$ is the stacked vector of bias currents, and $(\mathbf{i}_t)_{\text{net}} = \left[\ \mathbf{i}_t^n\ \right]^T \in \mathbb{R}^{2N\times 1}$ is the stacked vector of modulatory signals applied to the nodes and their sub-populations. Finally, $\overline{\mathbf{F}}_{\text{net}}(\mathbf{u}_{\text{net}}, \boldsymbol{\sigma}_{\text{net}}) = \left[\ \overline{\mathbf{F}}(\mathbf{u}^n, \boldsymbol{\sigma}^n)\ \right]^T \in \mathbb{R}^{2N\times 1}$ is the stacked vector of mean-field non-linear neuronal functions.

## 2.1. Mathematical modeling assumptions

The following assumptions were made during the mathematical modeling process.

- We assume that the properties of underlying microcircuits of each macro-scale node, including their geometric connectivity and coupling, are unknown, except the overall diversity of neuronal excitability parameterized by $\boldsymbol{\sigma}^n\ \forall\ n \in [N]$, and the intra-population connectivity defined in $\mathbf{W}$.
- Following prior work on whole-brain networks [52], we ignore time delays between the nodes.
- We assume that only a subset of macro-scale network nodes is influenced by external stimulation. This approach contrasts with neuronal-level network analyses, where stimulation is often applied more broadly across all nodes in the network [14,16,20]. Given the spatial distribution of brain regions, it's improbable that all areas are simultaneously affected. Unstimulated nodes are biased toward a critical state, where their stability is influenced only by intrinsic excitability heterogeneity and the dynamics shared through coupling with other nodes. We further assume that the stimulation is applied only to the excitatory sub-populations following [14]. This means that $\mathbf{i}_t^n$ can be expressed as:

$$\mathbf{i}_t^n = \begin{cases} [I_{\text{e}}^n,\ 0]^T & \text{if } n \in \mathcal{I}_M \\ [0,\ 0]^T & \text{otherwise,} \end{cases} \quad (5)$$

  where $\mathcal{I}_M \subset [N]$ is the set of indices of the modulated nodes of the network.
- We assume other parameters of the model to be constant: $\mathbf{T}^n = \mathbf{T},\ \mathbf{i}_0^n = \mathbf{i}_0$, and $\mathbf{W}^n = \mathbf{W}\ \forall n \in [N]$. This means that network parameters are not changing except $\boldsymbol{\sigma}^n$ and $K_{\text{glob}}$ for each simulation setup.

Following the above assumptions, Table 1 summarizes the values of the parameters used for simulations. The constant parameters are selected following [14] that are based on previous work on oscillatory cortical networks [53–56].

## 2.2. Measuring system behavior

As we model the brain at the macro-scale, measures defined for micro-scale neural networks are inapplicable – since we do not have access to underlying neuronal firing activities. Instead, we use the following measures to derive insights into the effect of excitability heterogeneity and the global coupling parameter on the stability and trivialization of the macro-scale brain network model.

**Table 1. Key parameters.**

| Parameter | Symbol | Value |
|---|---|---|
| Excitatory time constant | $\tau_e$ | 10 ms |
| Inhibitory time constant | $\tau_i$ | 5 ms |
| Non-linear gain of activation function | $\beta$ | 4.8 |
| Excitatory bias current | $I_{e,0}$ | -15.625 mV |
| Inhibitory bias voltage | $I_{i,0}$ | -31.25 mV |
| Stimulation | $I_e^M$ | Variable |
| Excitatory-excitatory synaptic strength | $w_{ee}$ | 100 |
| Excitatory-inhibitory synaptic strength | $w_{ei}$ | 187.5 |
| Inhibitory-excitatory synaptic strength | $w_{ie}$ | -293.75 |
| Inhibitory-inhibitory synaptic strength | $w_{ii}$ | -8.125 |
| Excitatory heterogeneity | $\sigma_e$ | Variable |
| Inhibitory heterogeneity | $\sigma_i$ | Variable |
| Time step | $\Delta t$ | 0.05 ms |
| Simulation time | $T$ | 2500 ms |
| Settling time | $t_s$ | 500 ms |
| Global synaptic coupling parameter | $K_{glob}$ | Variable |
| Structural connectivity weights | $p_{nm}$ | Variable |

https://doi.org/10.1371/journal.pcsy.0000057.t001

**2.2.1. Lyapunov stability.** We use temporally averaged Lyapunov exponents to estimate the Lyapunov stability of the macro-scale brain network using neural dynamics of the E sub-population of each brain region. In the context of brain activity, Lyapunov stability implies that the brain can maintain a stable state after experiencing either intrinsic or extrinsic stimulation [57]. Since the E sub-populations are stimulated in our model and directly affect overall network stability in terms of electrophysiological activity [6], our analysis on stability focuses only on these sub-populations. To evaluate their stability, we compute the Lyapunov exponents for the one-dimensional time series of the E sub-population at each node $n \in [N]$, denoted by $\ell_e^n$. Following [58], the Lyapunov exponents are computed as:

$$\ell_e^n = \frac{1}{T - t_s - 1} \sum_{k=1}^{T-t_s} \log\left( \left| u_e^n[t_k] - u_e^n[t_k - 1] \right| \right). \tag{6}$$

This calculation measures the local stability of the E sub-population dynamics by determining the separation rates of nearby points along the real line [16,58,59]. The Lyapunov exponents are undefined for systems where the differential is zero, i.e., systems without fluctuations or those in a saturated state [58]. Such system states are classified as supercritical stable regions. The parameters used in Eq (6) correspond to those listed in Table 1.

Instead of using the maximum Lyapunov exponent, we focus on the temporally averaged Lyapunov exponent, which reflects stability as an average measure over time rather than a marker of the overall dynamic state. A negative $\ell_e^n$ indicates that the node maintains relative stability with slow dynamics, while a positive value points to large, rapid fluctuations, signaling instability. Additionally, $\ell_e^n \approx 0$ suggests the presence of oscillatory dynamics. We define the Lyapunov stability of the network as $\ell_e^n$ averaged across the nodes in $\mathcal{I}_M$:

$$\bar{\ell}_e = \frac{1}{|\mathcal{I}_M|} \sum_{n \in \mathcal{I}_M} \ell_e^n. \tag{7}$$

**2.2.2. System resilience and multi-stable region emergence.** Although the network dynamics defined in Eq (4) are nonlinear, we can analyze local system behavior by linearizing

the system around its equilibria. Consider a constant modulatory signal $I_e^M \in [0, 31.25]$ mV applied on nodes $n \in \mathcal{I}_M$. Given $\boldsymbol{\sigma}_{\text{net}}, K_{\text{glob}}$, and $\mathbf{P}$, we numerically compute the singular points of the system $\mathcal{U}_{I_e^M} := \{\overline{\mathbf{u}}_{\text{net}}^l\}$ using Powell's algorithm [60]. We linearize the system around each $\overline{\mathbf{u}}_{\text{net}}^l \in \mathcal{U}_{I_e^M}$ using the Jacobian matrix $\mathbf{J} \in \mathbb{R}^{2N \times 2N}$, defined as:

$$\mathbf{J}\left(\overline{\mathbf{u}}_{\text{net}}^l; \mathbf{P}, \boldsymbol{\sigma}_{\text{net}}, K_{\text{glob}}\right) = \mathbf{T}_{\text{net}}\left(K_{\text{glob}}\mathbf{P}_{\text{net}} - \mathbb{I}_{2N} + \mathbf{W}_{\text{net}}\overline{\mathbf{R}}_{\text{net}}(\overline{\mathbf{u}}_{\text{net}}^l, \boldsymbol{\sigma}_{\text{net}})\right), \tag{8}$$

where $\overline{\mathbf{R}}_{\text{net}}(\overline{\mathbf{u}}_{\text{net}}^l, \boldsymbol{\sigma}_{\text{net}}) \in \mathbb{R}^{2N \times 1}$ is the stacked vector of vectorized susceptibility function $\overline{\mathbf{R}}(\overline{\mathbf{u}}^{l,n}, \boldsymbol{\sigma}^n)$ for $n \in [N]$ and $l \in [\,L\,]$ where $L = |\mathcal{U}_{I_e^M}|$. The vectorized susceptibility function $\overline{\mathbf{R}} : \mathbb{R}^4 \to \mathbb{R}^2$ is described by $\overline{\mathbf{R}}(\mathbf{x}, \mathbf{s}) = \left[R_\beta(x_1, s_1), R_\beta(x_2, s_2)\right]^T \in \mathbb{R}^2$ where $R_\beta(x, s)$ is defined as:

$$R_\beta(x, s) = \int_{-\infty}^{\infty} \frac{\beta \exp(-\beta(x+\theta))}{\left[1 + \exp(-\beta(x+\theta))\right]^2} \rho(\theta; s) d\theta. \tag{9}$$

As $s = \sigma_{e,i}$ increases, the susceptibility of the neuronal population reduces significantly. For systems with multiple fixed points i.e., $\left|\mathcal{U}_{I_e^M}\right| > 1$, Eq (8) is evaluated for each fixed point yielding a set of Jacobian matrices.

We compute the eigen-decomposition of the Jacobian matrices for each $\overline{\mathbf{u}}_{\text{net}}^l \in \mathcal{U}_{I_e^M}$ to understand the system's local behavior around that singular point. We define the eigen spectrum for $\overline{\mathbf{u}}_{\text{net}}^l$ as $\Lambda^l = [\lambda^{l,1}, \lambda^{l,2}, \ldots, \lambda^{l,2N}]^T \in \mathbb{C}^{2N \times 1}$ where the $\lambda^{l,k} = a^{l,k} + jb^{l,k} \in \mathbb{C}$ are the eigenvalues. Table 2 characterizes various possible system behaviors.

S1 Appendix provides additional details on computing $\overline{\mathbf{u}}_{\text{net}}^l$, deriving $\mathbf{J}$ and determining the system behavior. As each $\overline{\mathbf{u}}_{\text{net}}^l \in \mathcal{U}_{I_e^M}$ is a $\mathbb{R}^{2N}$ vector, we apply Kernel PCA [61] to reduce its dimensionality to $\mathbb{R}$ for visualization. We define $\Psi : \mathbb{R}^{2N} \to \mathbb{R}$ as the Kernel PCA operation applied on each equilibria in $\mathcal{U}_{I_e^M}$. Further details are provided in S2 Appendix.

Further, we define the system's dampening rate $\zeta^l$ and oscillatory rate $\omega^l$ for each singular point $\overline{\mathbf{u}}_{\text{net}}^l$ from $\Lambda^l$. We define $\zeta^l = \max_{k \in [2N]} \{a^{l,k}\}$ as the maximal real part of the eigenspectrum $\Lambda^l$ i.e., of the dominant eigenvalue. This parameter determines overall system stability. We define the two dominating oscillatory rates (i.e., eigenfrequencies) from the two largest mean adjusted-eigenvalues i.e., $\tilde{\lambda}^{l,k} = \lambda^{l,k} - \langle \lambda^{l,k} \rangle_k$, as $\omega_1^l = \frac{\tilde{b}^{l,1}}{2\pi}$, and $\omega_2^l = \frac{\tilde{b}^{l,2}}{2\pi}$ where $\tilde{b}^{l,\cdot} = \Im\{\tilde{\lambda}^{l,\cdot}\}$ and $\langle \lambda^{l,k} \rangle_k = \frac{1}{2N} \sum_{k=1}^{2N} \lambda^{l,k}$.

We define multi-stable regions as the intervals of $I_e^M$ where $\left|\mathcal{U}_{I_e^M}\right| > 1$ for each $I_e^M$ in the interval. These regions indicate the presence of multiple steady-state points and a propensity for bifurcations as external stimulation changes. This implies that the system will have at least one equilibrium point $\overline{\mathbf{u}}_{\text{net}}^l \in \mathcal{U}_{I_e^M}$ where $\zeta^l > 0$. Such occurrences suggest reduced resilience to external disturbances, as highlighted by [17], making system control more challenging. Thus,

**Table 2. Determining local system stability based on eigenvalues of the locally linearized system.**

| Stable state | Stability criteria | | Color |
|---|---|---|---|
| | $a^{l,k} = \Re\{\lambda^{l,k}\}$ | $b^{l,k} = \Im\{\lambda^{l,k}\}$ | |
| Stable spiral | $a^{l,k} < 0 \; \forall \; k \in [2N]$ | $\exists b^{l,k}$ s.t. $b^{l,k} \neq 0$ | Brown |
| Stable node | $a^{l,k} < 0 \; \forall \; k \in [2N]$ | $b^{l,k} = 0 \; \forall \; k \in [2N]$ | Green |
| Centre | $a^{l,k} = 0 \; \forall \; k \in [2N]$ | $b^{l,k} = 0 \; \forall \; k \in [2N]$ | Black |
| Unstable spiral | $a^{l,k} > 0 \; \forall \; k \in [2N]$ | $\exists b^{l,k}$ s.t. $b^{l,k} \neq 0$ | Purple |
| Unstable node | $a^{l,k} > 0 \; \forall \; k \in [2N]$ | $b^{l,k} = 0 \; \forall \; k \in [2N]$ | Blue |
| Saddle Point | $\exists a^{l,k}$ s.t. $a^{l,k} > 0$ | $b^{l,k} = 0 \; \forall \; k \in [2N]$ | Red |

https://doi.org/10.1371/journal.pcsy.0000057.t002

we define the system as resilient only if $\zeta^l < 0\ \forall l \in [\,L\,]$ for a given $I_e^M$. We use $\Delta I_e^M$ to quantify the width of these multi-stable regions, reflecting the range of modulatory signal amplitudes over which multi-stability persists. This measure helps us understand how excitability heterogeneity and the global coupling parameter affect the system's resilience against external disturbances.

## 3. Numerical results using a two-node macro-scale brain network

This section presents numerical results using a coupled two-node macro-scale network. In Sect 3.1, we investigate how the interplay between intrinsic excitability heterogeneity and synaptic coupling gain affects the stability of macro-scale neural dynamics, particularly within the E sub-populations. Sect 3.2 delves deeper, examining the differential impact of excitatory and inhibitory heterogeneity on the stability of the stimulated node in the network. Finally, in Sect 3.3, we explore how excitability heterogeneity contributes to the emergence of multi-stable regions and the resilience of the system at each equilibrium as the stimulation varies. While limited in scope, a two-node network provides valuable insights into how intrinsic excitability heterogeneity functions within a broader spatial scale.

In accordance with Sect 2.1, let $\mathbf{P} \in \mathbb{R}^{2\times 2}$ denote the normalized connectome, where $p_{nm} = 1$ for $n \neq m$ and $n, m \in [2]$. The parameter $K_{\text{glob}}$ is varied within the interval $[-1,1)$ to model both excitatory ($K_{\text{glob}} > 0$) and inhibitory ($K_{\text{glob}} < 0$) inter-regional coupling. We observed that when $K_{\text{glob}}$ exceeds the range of $[-1,1)$ the macro-scale neural dynamics, especially within E sub-populations, become unbounded. Consequently, we confine the range of $K_{\text{glob}}$ in our simulations to $[-1,1)$. We apply a temporally constant stimulus $I_e^1 \in [0, 31.25]$ mV to the E sub-population of node 1. We simulate a scenario where a brain region is stimulated while another remains unstimulated. This approach is relevant to the spatial scale considered and offers clinical value by revealing how information and seizure-like dynamics propagate from the onset region to other brain areas. The two-node brain network is illustrated in Fig 2.

We consider 2 main configurations for setting the heterogeneity parameters of the two nodes in the brain network.

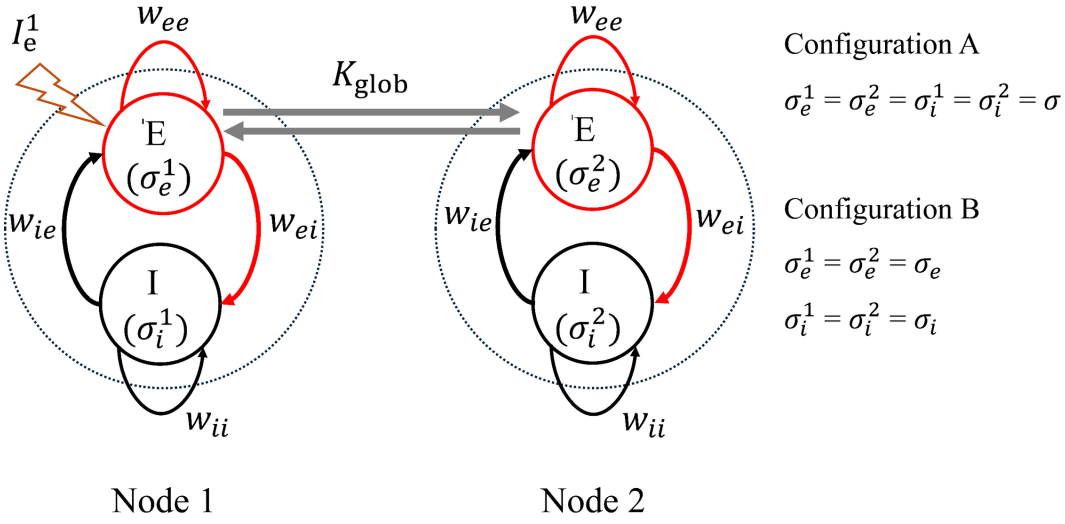


**Fig 2. Two nodes macro-scale brain network.** The E sub-population of node 1 is stimulated by a constant external signal amplitude $I_e^1$.

https://doi.org/10.1371/journal.pcsy.0000057.g002

1. Uniform heterogeneity configuration ($\mathcal{C}$–A): We consider the situation where we set the excitability heterogeneity of both nodes and sub-populations to be equal i.e., $\sigma = \sigma_e^n = \sigma_i^n \; \forall \; n \in [2]$. Here, we change the heterogeneity of both sub-populations of the two nodes simultaneously. This reduces the parameter space to $(K_{glob}, \sigma)$ for a given $I_e^1$.
2. Differential heterogeneity configuration ($\mathcal{C}$–B): Here we denote excitability heterogeneities of the sub-populations of the nodes using two independent parameters: $\sigma_e = \sigma_e^1 = \sigma_e^2$ and $\sigma_i = \sigma_i^1 = \sigma_i^2$. This increases the variable parameter space to $(K_{glob}, \sigma_e, \sigma_i)$ for a given $I_e^1$.

As detailed in Table 1, simulations were run for $T = 2500$ ms with an adaptive solver period of $t_s = 500$ ms to ensure stability. The dynamics in Eq (4) were solved using the Euler-Maruyama method, suitable for stochastic differential equations. Independent Gaussian noise with variance $D_0$ was introduced but had minimal impact on the results (S3 Appendix). Therefore, simulations were run with $D_0 = 0.0$ i.e., without external noise. Results were averaged over 10 trials to eliminate dependence on initial conditions.

## 3.1. Excitability heterogeneity and the synaptic coupling collectively achieve stability in macro-scale neural dynamics

Our first step is to understand the effect of the underlying excitability heterogeneity on the Lyapunov stability of a macro-scale brain network with a stimulated brain region. Using $\mathcal{C}$–A, we change the heterogeneity of the sub-populations of the two nodes simultaneously. The computational study shows that an increased excitability heterogeneity achieves stability for a given synaptic coupling gain. However, for a constant stimulation $I_e^1$, the required level of excitability heterogeneity to stabilize the system varies depending on whether the inter-regional coupling is excitatory or inhibitory. The results are summarized in Fig 3.

Fig 3a shows the behavior of $\bar{\ell}_e$ as a function of $K_{glob}$ for both homogeneous ($\sigma = 2.5$) and heterogeneous ($\sigma = 16.5$) networks under constant stimulation. In the homogeneous network with lower $\sigma$, instability persists until the synaptic coupling between the stimulated and unstimulated nodes becomes excitatory and sufficiently large ($K_{glob} \geq 0.8$). In contrast, the heterogeneous network with higher $\sigma$ remains stable with $\bar{\ell}_e < 0$ across the entire range of $K_{glob}$.

As each sub-population becomes homogeneous (i.e., lower $\sigma$), the resulting dynamics are reduced. This is because the mean-field firing function $F_\beta(\cdot, \cdot)$ of the brain model, shown in Fig 1, becomes steeper as the variability in firing thresholds decreases, limiting high-firing responses to only higher pre-synaptic neural inputs [26]. Previous studies [13,20] show that this reduced variability in I sub-populations weakens intra-node negative feedback, thereby diminishing local feedback inhibition within the E sub-populations. As a result, the system becomes more susceptible to external stimulation, with excitatory activity primarily driven by external stimulation and the coupling between regions.

As heterogeneity within each node's sub-populations increases, the population response function becomes less steep, spreading across a wider range of pre-synaptic neural inputs, as suggested by previous studies [13,26]. This results in lower output rates for higher pre-synaptic inputs, while increasing the firing rate for lower pre-synaptic inputs. When $|w_{ie}| > w_{ee}$, higher firing rates in the I sub-populations enhance feedback inhibition to the E sub-populations, resulting in stronger inhibition of excitatory activity. Simultaneously, the reduced firing rates for higher pre-synaptic inputs in the E sub-population decrease excitatory activity, helping to stabilize the system against external stimulation. If inter-node coupling

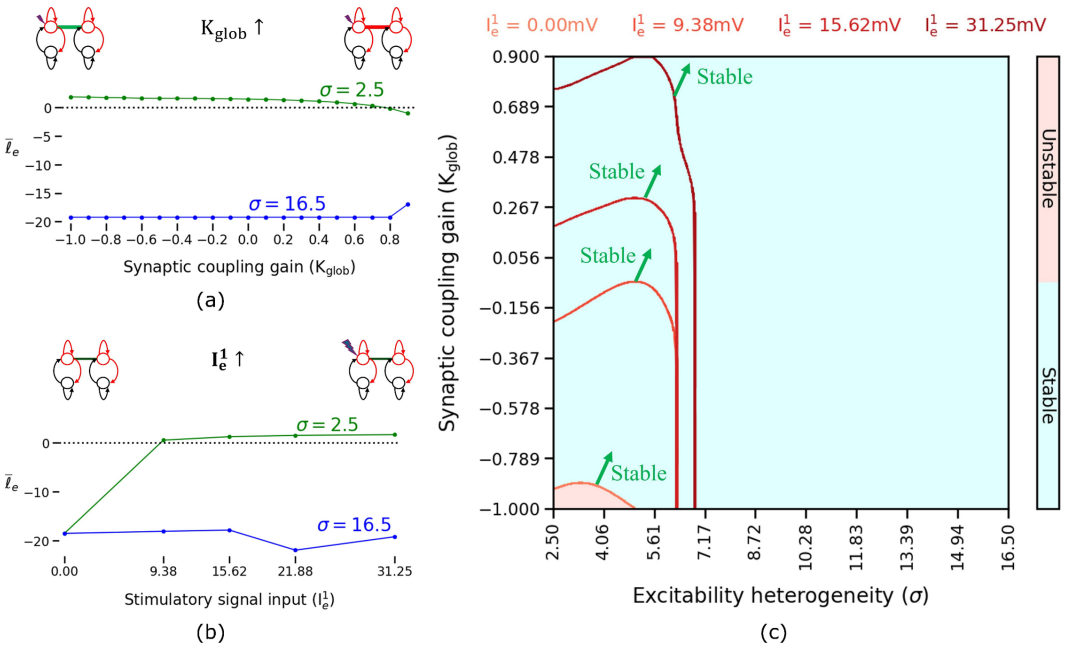


**Fig 3. Excitability heterogeneity, in combination with inter-node synaptic coupling, collectively achieves Lyapunov stability against external stimulation at the macro-scale.** Sub-figure (a) shows how the stability of a homogeneous and heterogeneous network changes with $K_{glob}$. The heterogeneous network maintains stability irrespective of the coupling between the two regions. The results are for $I_e^1$ = 31.25 mV. Sub-figure (b) shows that a homogeneous network becomes unstable even at lower external stimulation. The results correspond to $K_{glob}$ = −0.4. Sub-figure (c) shows how the parameter manifolds in ($K_{glob}$, $\sigma$) space change for different $I_e^1$. The shaded red area indicates the region of instability for $I_e^1$ = 0.0 mV, while the green arrows at each boundary point towards stable regions.

https://doi.org/10.1371/journal.pcsy.0000057.g003

is excitatory i.e., $K_{glob} > 0$, this increased local inhibition is shared across nodes, contributing to stability. Conversely, if the coupling is inhibitory i.e., $K_{glob} < 0$, it reverses the feedback effect, leading to bursting-type dynamics within the E sub-population and causing network instability.

Fig 3b shows that homogeneous networks are unstable even with smaller external stimulations, whereas heterogeneous networks remain stable within the stimulation range considered. This indicates that without heterogeneity, the network is prone to bifurcations under lower amplitude stimulations. Fig 3c presents parameter manifolds in $(K_{glob}, \sigma)$ space for different stimulations. As heterogeneity increases, the network becomes less dependent on synaptic coupling. While higher stimulation slightly increases excitability heterogeneity required to maintain stability, this effect is marginal. However, as the stimulation continues to increase, the region of instability grows, and the increased excitatory coupling becomes less sufficient to stabilize the systems with lesser heterogeneity. When $K_{glob} \approx 1$, the network stabilizes regardless of heterogeneity because the model's dynamics become saturated. However, such saturated dynamics do not reflect physiological brain activity [62,63].

This confirms that the excitability heterogeneity of the underlying neuronal populations influences the stability of macro-scale neural dynamics. Moreover, it highlights how excitability heterogeneity serves as an intrinsic control mechanism for the macro-scale dynamics in a stimulated system, extending the micro-scale findings reported in [16]. Further, coupling with an unmodulated node provides sufficient neural feedback to support the stabilization process.

### 3.2. Excitatory and inhibitory heterogeneity have differential effects on the stability of macro-scale dynamics

After establishing the effect of excitability heterogeneity on the stability of the macro-scale neural dynamics, an intriguing question arises: what occurs when the two sub-populations in each node have relatively different levels of heterogeneity? To address this question, we follow $\mathcal{C}$–B. By fixing the heterogeneity of the E (or I) sub-populations, we investigate how the heterogeneity of the I (or E) sub-population influences the stability of the macro-scale neural dynamics. Our investigation reveals that inhibitory heterogeneity plays an important role in stabilizing a stimulated macro-scale network. While excitatory heterogeneity assists the stabilization, it alone is insufficient for stability. The findings are summarized in Fig 4.

We depict the change in $\bar{\ell}_e$ with $K_{glob}$ considering four permutations of heterogeneity in the E and I sub-populations in Fig 4a. We observe that networks with homogeneous I sub-populations (i.e., blue and red curves) fail to achieve stability in their stimulated node, even with stronger excitatory coupling (i.e., $K_{glob} = 0.8$). A network with heterogeneous E sub-population and homogeneous I sub-population (red curve) exhibits slightly higher positive $\bar{\ell}_e$ particularly for excitatory coupling than a network with both sub-populations being homogeneous (blue curve), indicating greater instability. As coupling becomes more excitatory, $\bar{\ell}_e$ decreases in both cases. However, the stimulated macro-scale node remains unstable with $\bar{\ell}_e \geq 0$.

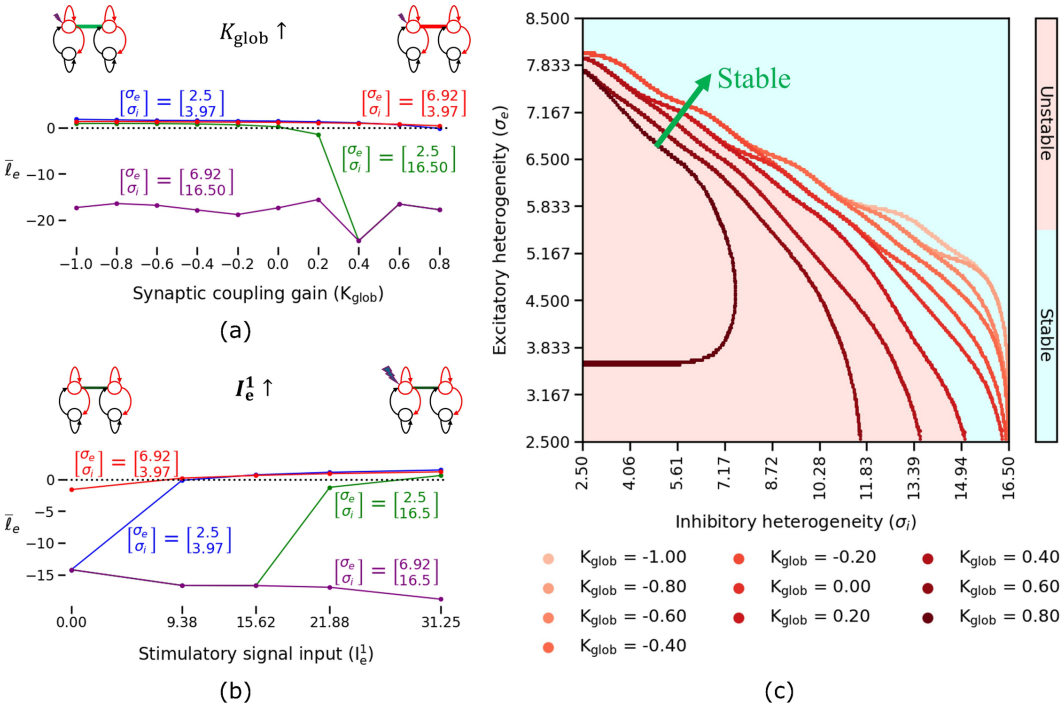


**Fig 4. Excitatory and inhibitory heterogeneity exert distinct effects on the stability of macro-scale neural dynamics.** Sub-figure (a) shows how the stability of networks with varied heterogeneity in E and I sub-populations changes with $K_{glob}$. Sub-figure (b) shows that when the network loses heterogeneity in one or both sub-populations, it becomes vulnerable even to weaker external stimulations. These results are depicted for $K_{glob} = -0.2$. Sub-figure (c) displays the parameter manifolds in $(\sigma_e, \sigma_i)$ space for different $K_{glob}$. The shaded red region corresponds to the unstable region of $K_{glob} = 0.2$, while the green arrow at each boundary point is towards stable regions. All results in this figure are associated with $I_e^1 = 31.25$ mV.

https://doi.org/10.1371/journal.pcsy.0000057.g004

This instability arises because local feedback inhibition on excitatory activities decreases at each macro-scale node. This is caused by a significant reduction in neural activity within homogeneous I sub-populations as their response function contracts. For example, in Fig 5a, the mean-field response function for the homogeneous I sub-population with $\sigma_i = 3.92$ is nonzero only for significantly higher thresholds. The corresponding time series reveal substantial amplitude fluctuations in the excitatory dynamics. Excitatory activity drops to a minimum when $u_i^1 \geq -10$ and reaches a peak when the inhibitory input is at its lowest, suggesting that the dynamics of the homogeneous I sub-population is strongly driven by excitatory input. Figs A and B in S6 Appendix further support this behavior, showing that the low heterogeneity in the E and I sub-populations under high stimulation drives the system into a regime of large limit cycles. This leads to abrupt transitions in network activity, as seen in Fig 5a. Thus, as detailed in Sect 3.1 and illustrated in Fig C of S6 Appendix, with homogeneous E and I sub-populations, the Lyapunov stability of the system depends largely on the applied stimulus and the coupling between regions.

As inhibitory heterogeneity increases while E sub-populations remain homogeneous, the network stability improves, as shown in Fig 5b and 5c. For $\sigma_i = 14$, the response function of the I sub-populations demonstrates higher firing rates even at lower pre-synaptic activity levels. This enhances the smoothing of excitatory activity fluctuations by increasing local inhibitory feedback. However, the network remains unstable due to persistent fluctuations

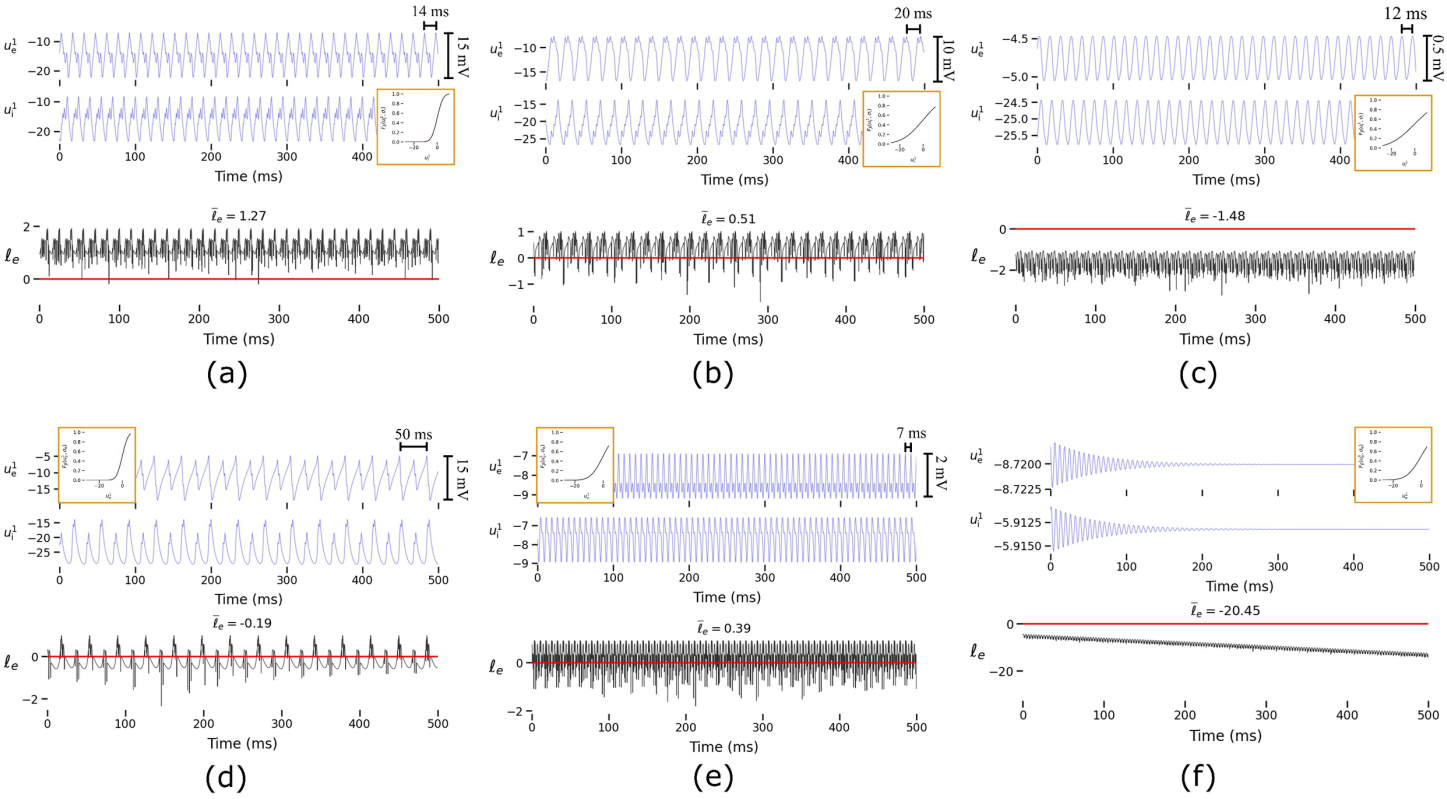


**Fig 5. Temporal fluctuations of excitatory and inhibitory neural dynamics of the two-node macro-scale brain network.** Each sub-figure depicts the temporal dynamics of E and I sub-populations of the stimulated node (top panel) and the temporal fluctuations of the corresponding Lyapunov exponents (bottom panel). Sub-figures (a)–(c) show results for $K_{glob} = 0.2$: (a) $\sigma_e = 2.5$, $\sigma_i = 3.97$; (b) $\sigma_e = 2.5$, $\sigma_i = 14.0$; (c) $\sigma_e = 2.5$, $\sigma_i = 16.5$. Sub-figures (d)–(f) show results for $K_{glob} = 0.8$: (d) $\sigma_e = 2.5$, $\sigma_i = 3.97$; (e) $\sigma_e = 6.92$, $\sigma_i = 3.97$; (f) $\sigma_e = 8.0$, $\sigma_i = 3.97$. All simulations were conducted with $I_e^1 = 31.25$ mV.

https://doi.org/10.1371/journal.pcsy.0000057.g005

in amplitude in excitatory activity despite a reduction in $\bar{\ell}_e$. This behavior aligns with the bifurcation results observed in S6 Appendix. When $\sigma_i$ increases with homogeneous E sub-populations, the system approaches the Hopf bifurcation curve, as observed in Fig C(c) of S6 Appendix. Although the limit cycle contracts, excitatory amplitude fluctuations persist, resulting in positive $\bar{\ell}_e$. When inhibitory heterogeneity increases further to $\sigma_i = 16.5$, the system crosses the Hopf bifurcation curve and enters a stable equilibrium regime, as shown in Fig C(c) of S6 Appendix. At this point, the inhibitory contribution becomes strong enough to suppress excitatory activity, leading to a marked improvement in network stability.

While high inhibitory heterogeneity can stabilize the network, this effect depends strongly on the nature of the coupling between regions. As shown in Fig 4a, networks with excitatory coupling ($K_{glob} > 0$) can better withstand stronger external stimulation when inhibitory heterogeneity is high (green curve). However, when the coupling becomes inhibitory ($K_{glob} < 0$), the dynamics change fundamentally. With $K_{glob} < 0$, local dynamics at a brain region are inverted (i.e., a phase shift of 180 degrees) when propagated to other brain regions. As a result, any decrease in excitatory neural activity caused by increased local inhibition is transferred to other regions as an increase in excitatory activity, amplifying fluctuations and destabilizing the stimulated network. This behavior is evident in Fig 5, where reducing the coupling strength from $K_{glob} = 0.8$ (Fig 5d) to $K_{glob} = 0.2$ (Fig 5a) results in high-amplitude fluctuations and a positive Lyapunov exponent, which indicates instability. This transition is further supported by the bifurcation structure in Fig C(a) in S6 Appendix, where decreasing $K_{glob}$ moves the system across the multi-stable region, giving rise to a limit cycle and the resulting abrupt transitions. This instability can be mitigated by increasing excitatory heterogeneity, as shown by the purple curve in Fig 4a. Greater diversity in the E sub-populations provides a balancing mechanism against the increased negative feedback from the I sub-populations. This reduces the shared excitatory-like dynamics between regions, particularly when $K_{glob} < 0$, as it inverts the signals from the E sub-populations. Thus, with adequate heterogeneity in both sub-populations, the network maintains stability even under stronger external stimulation across the entire range of coupling considered.

Moreover, increasing excitatory heterogeneity while keeping the I sub-populations homogeneous leads to network instability. As excitatory activity increases, the lack of sufficient local inhibitory feedback prevents the system from stabilizing under external stimulation. This instability is evident in Fig 5e, where high excitatory heterogeneity ($\sigma_e = 6.92$) leads to fast, high-amplitude ripples and rapid state transitions, resulting in a positive $\bar{\ell}_e$. In contrast, lower excitatory heterogeneity ($\sigma_e = 2.5$) produces slower, smaller oscillations, as shown in Fig 5d, with a negative Lyapunov exponent reflecting stability. However, further increases in $\sigma_e$ elevate mean inhibitory activity to a regime where the response function of the homogeneous I sub-populations provides higher firing rates, as seen in Fig 5f. This balance between excitatory and inhibitory activities dampens oscillations, stabilizing the network (see Fig C(b) in S6 Appendix).

Networks with homogeneous sub-populations are unstable at weaker stimulation, as shown in Fig 4b. Specifically, networks with homogeneous I sub-populations (blue and red curves) are more prone to instability than those with higher inhibitory heterogeneity (green and purple curves). Furthermore, systems with high excitatory heterogeneity and low inhibitory heterogeneity (red curve) become less stable with less negative $\bar{\ell}_e$ even without a stimulation ($I_e^1 = 0\,\mathrm{mV}$). This indicates that excitatory heterogeneity alone is insufficient to stabilize the system without accompanying inhibitory heterogeneity.

In Fig 4c, we observe distinct parameter manifolds in $(\sigma_e, \sigma_i)$ space for different $K_{glob}$. Similar depictions for various modulatory signal strengths are shown in S4 Appendix. When $K_{glob} \simeq -1$, high inhibitory heterogeneity is required to stabilize the network. As $K_{glob}$

becomes more positive, the unstable region in parameter space shrinks, with inhibitory heterogeneity playing a larger role than excitatory heterogeneity. For example, at $K_{glob} = 0.8$, the unstable region is limited to $\sigma_i < 8$, while changes in excitatory heterogeneity have a marginal effect. Conversely, lower excitatory heterogeneity can be stabilized with sufficient inhibitory heterogeneity for a given $K_{glob}$. With extreme excitatory heterogeneity ($\sigma_e > 8$), the system stabilizes regardless of inhibitory heterogeneity or coupling. This occurs because high excitatory heterogeneity increases excitatory activity enough to drive inhibitory populations above their firing threshold, balancing the excitatory-inhibitory dynamics. As seen in Fig 5c, for $\sigma_e = 8$, the stimulated region shows decaying oscillations with small amplitudes.

This demonstrates that excitatory and inhibitory heterogeneity differentially affect the Lyapunov stability of the perturbed node in the network. Notably, our results show that the inhibitory heterogeneity required to achieve stability changes with the coupling gain parameter while the excitatory heterogeneity changes marginally. Specifically, systems with excitatory heterogeneity but lacking inhibitory heterogeneity are often more unstable than those with homogeneous E sub-populations.

### 3.3. Excitability heterogeneity trivializes macro-scale brain network and improves resilience

Finally, we examine how excitability heterogeneity affects the emergence of multiple equilibria and resilience against external stimulations in the network, following Sect 2.2.2. Using $\mathcal{C}$–A, we found that excitability heterogeneity reduces the emergence of multiple equilibria as $I_e^1$ increases, thereby decreasing multi-stable regions. Additionally, higher heterogeneity improves the system's resilience to external stimulations, as quantified by $\zeta$. While $K_{glob}$ can enhance resilience by making the system more excitatory, it cannot fully stabilize the system without sufficient heterogeneity. These results are shown in Figs 6 to 10, where each sub-figure illustrates how dimension-reduced equilibrium points shift with $I_e^1 \in [0, 31.25]$ mV.

Subsequently, we explored whether a differential effect persists in trivialization and resilience enhancement when excitatory and inhibitory heterogeneity differs, using $\mathcal{C}$–B. We found that with adequate inhibitory heterogeneity, the system becomes trivialized and its resilience improves, regardless of excitatory heterogeneity and global coupling parameters. Notably, excitatory heterogeneity aids in trivialization, especially when homogeneous I sub-populations are present. However, as $K_{glob}$ becomes more excitatory, the system's dependence on excitatory heterogeneity diminishes. These results are shown in Figs 11 to 14.

In Fig 6a, multiple equilibria emerge in a homogeneous network as $I_e^1$ increases, each corresponding to stable states represented by different colors. As shown in the phase portraits in Fig 7b for $I_e^1 = 9.5$ mV, the neural dynamics converge to one of these stable states within the multi-stable region. These regions indicate bifurcation points, where system states shift from stable (green) to unstable (purple) as $I_e^1$ increases. A saddle-node bifurcation occurs, merging the stable node and saddle-node, resulting in a limit cycle around the unstable equilibrium, as seen in Fig 7c for $I_e^1 = 10.5$ mV. This represents a saddle-node invariant circle bifurcation, signifying a transition from a resting state to a seizure-like state as discussed in [64]. The time series shows stable oscillations within the limit cycle. As $I_e^1$ increases, the frequency of trajectories spiraling toward the limit cycle, denoted by $\omega$, also rises, as shown in Fig 7a. At $I_e^1 = 31.25$ mV (Fig 7d), both the oscillation frequency and amplitude of the limit cycle increase. Furthermore, the network's resilience, measured by $\zeta$ (defined in Sect 2.2), diminishes as $I_e^1$ increases as shown in Fig 6a. At $K_{glob} = 0.2$, the system remains resilient only for weaker stimulation ($I_e^1 < 5$ mV).

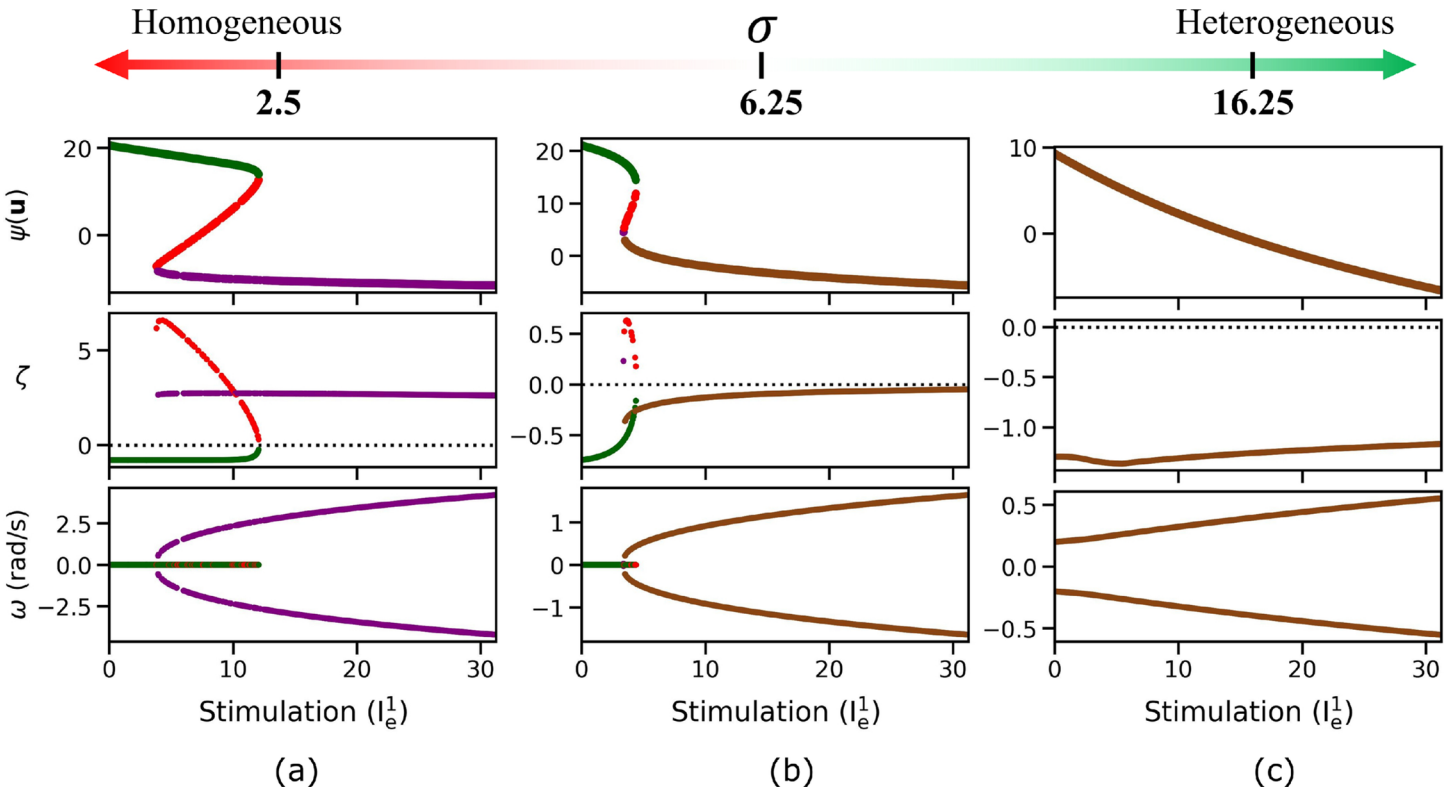


**Fig 6. Excitability heterogeneity trivializes two-node macro-scale brain network and achieves resilience against external stimulations.** The sub-figures labeled (a) to (c) each represent different heterogeneity values. Each sub-figure has three panels: (i) dimension-reduced equilibria with colors indicating stable states (Table 2), (ii) the maximum damping ratio $\zeta$, reflecting network resilience, and (iii) significant oscillatory rates $\omega$. All results are for $K_{glob} = 0.2$ and $\mathcal{C}$–A, with $\sigma_e = \sigma_i = \sigma$.

https://doi.org/10.1371/journal.pcsy.0000057.g006

Heightened heterogeneity reduces the occurrence of multi-stable regions and enhances resilience against external stimulations ($\zeta < 0$ for $I_e^1 \in [0, 31.25]$ mV), as shown in Fig 6b and 6c. Additionally, increased heterogeneity slows the oscillations ($\omega$), resulting in slower dynamics around the equilibria. As shown in Fig 8, for $\sigma = 6.25$, after the annihilation of the stable and saddle nodes, a stable spiraling equilibrium persists. For lower $I_e^1 = 5$ mV, the spiraling dynamics towards the equilibrium are characterized by the frequency $\omega$, as seen in Fig 8a. However, as $I_e^1$ increases, a small limit cycle emerges, illustrated in Fig 8b. This coexistence of a stable spiral equilibrium and a small-amplitude limit cycle in a high-dimensional system arises from the interaction between linear stability and nonlinear dynamics. While the equilibrium remains stable due to all eigenvalues having negative real parts (Fig 8c), the nonlinear terms generate a stable periodic orbit near the equilibrium as external stimulation increases. The small amplitude of the limit cycle suggests that the nonlinear driving terms are weak, and the system's high-dimensional nature compresses the oscillations to a localized region around the equilibrium. This phenomenon typically occurs near a bifurcation point; as shown in Fig 8c, increasing $I_e^1$ drives the complex eigenvalue pair closer to the real axis, sustaining smaller limit cycles around the equilibrium.

By comparing the evolution of equilibria in Fig 6a, 6b, and 6c, we observe that as $\sigma$ increases, the system transitions from an unstable spiral to a stable spiral with rising $I_e^1$. This indicates that for higher $I_e^1$, increased heterogeneity leads to the annihilation of the unstable spiral and stable limit cycle, resulting in an Andronov-Hopf bifurcation [65].

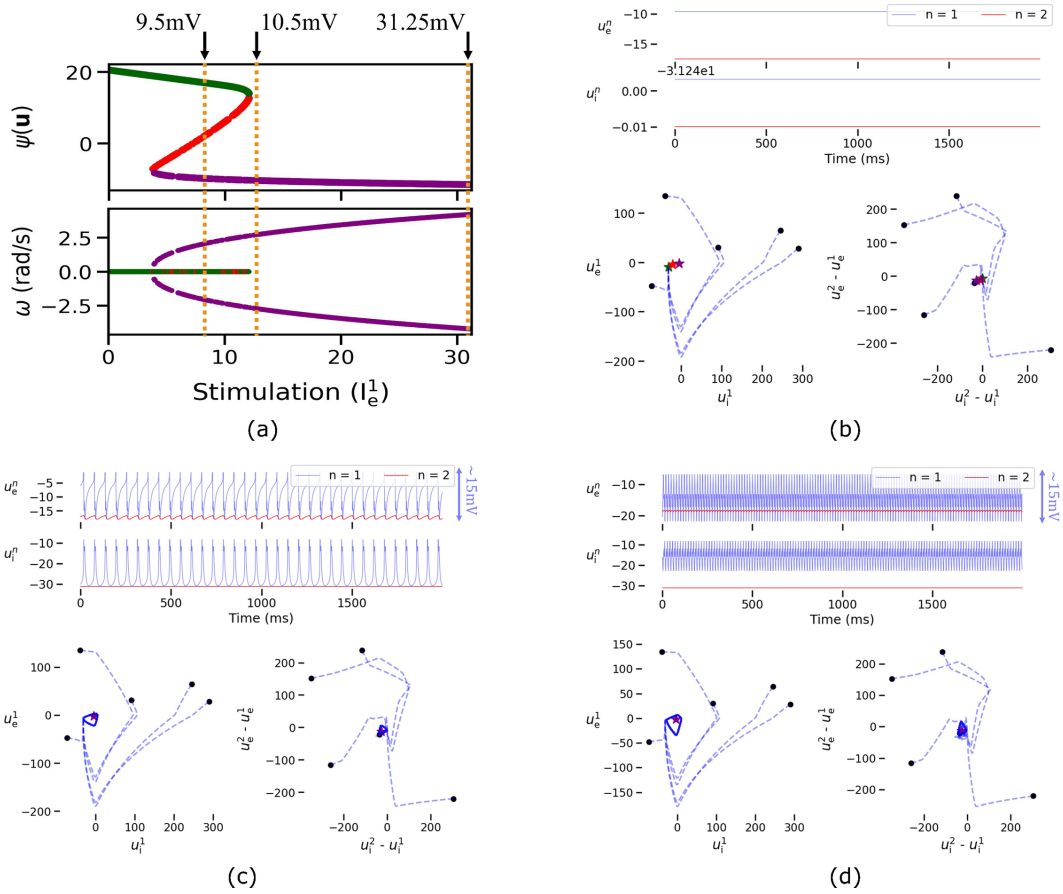


**Fig 7. Macro-scale dynamics at different $I_e^1$ values in Fig 6a.** Sub-figure (a) shows dimension-reduced equilibria from Fig 6a indicating the $I_e^1$ at which time series and phase portraits are illustrated. Sub-figures (b)–(d) display the time series (top) and 2D phase portraits (bottom) for node 1 and cross-node planes at (b) $I_e^1$ = 9.5 mV, (c) $I_e^1$ = 10.5 mV, and (d) $I_e^1$ = 31.25 mV. All figures are obtained with $\sigma_e = \sigma_i = 2.5$ and $K_{glob} = 0.2$.

https://doi.org/10.1371/journal.pcsy.0000057.g007

In Fig 9, we analyzed the impact of $K_{glob}$ on the emergence of multiple equilibria in a homogeneous network with $\sigma = 2.5$, focusing on trivialization and resilience. For inhibitory coupling ($K_{glob} < 0$), multiple equilibria persist across the stimulation range (Fig 9a and 9b), accompanied by high oscillations ($\omega \simeq \pm 5$ rad/s). Resilience is absent ($\zeta > 0$) for all inputs. Conversely, as coupling becomes excitatory, the system exhibits some trivialization and resilience at the macro-scale. Notably, with highly excitatory coupling (Fig 9d), the system gains resilience across a wide range of $I_e^1$, vulnerable only to extremely high inputs. This resilience is attributed to positive neural feedback between nodes, shifting the biased state of the nodes away from their critical state to a more stable state, requiring substantial positive stimulation to destabilize the system. This effect is also reflected in Fig C(a) in S6 Appendix, where increasing $K_{glob}$ shifts the bifurcation curves rightward along the $I_e^1$ axis. Despite $K_{glob}$'s less significant trivialization compared to neuronal heterogeneity, it enhances resilience, particularly with positive neural feedback shared between nodes.

We identified the manifold delineating system configurations with multi-stable regions from those with mono-stable regions as $I_e^1$ varies, as depicted in Fig 10. Particularly, multi-stable regions persist primarily in highly homogeneous networks under inhibitory coupling

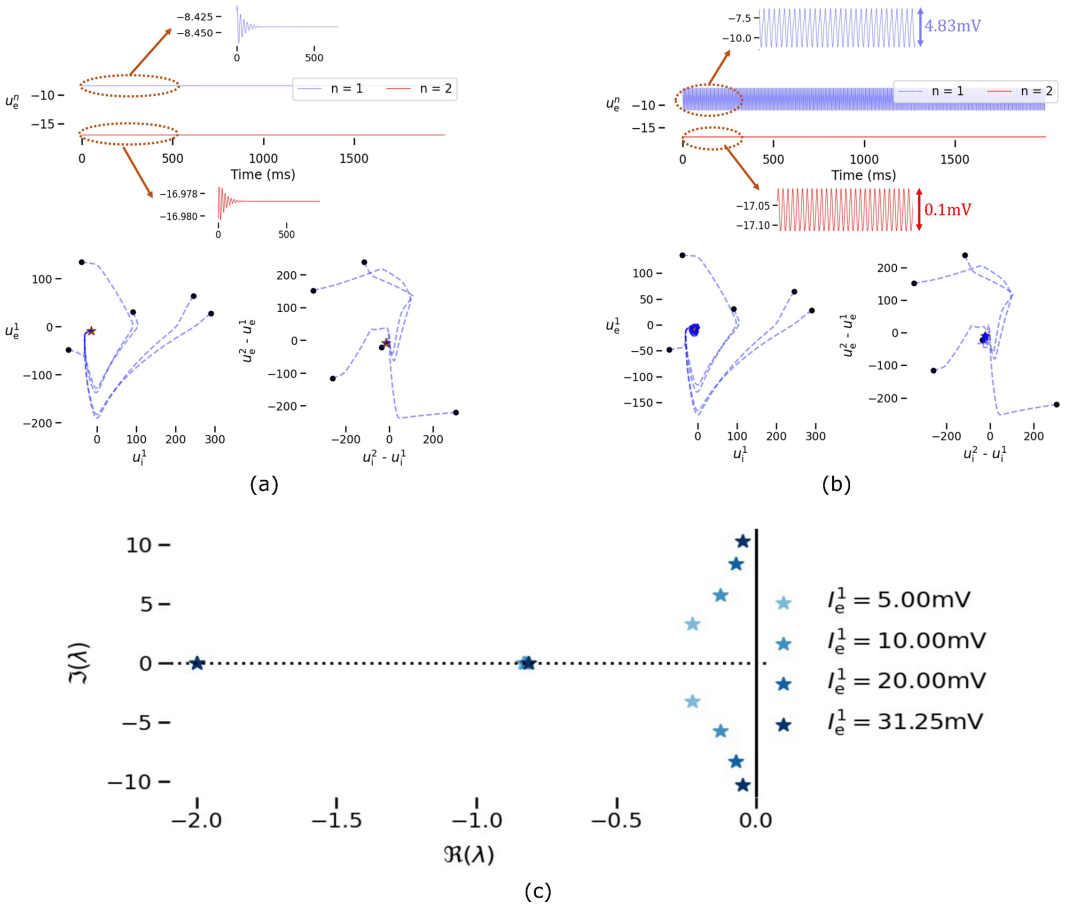


**Fig 8. Macro-scale dynamics at different $I_e^1$ values in Fig 6b.** Sub-figures (a) and (b) show 2D phase portraits on node 1 and cross-node planes for $I_e^1 = 5$ mV and $I_e^1 = 31.25$ mV, respectively. Sub-figure (c) shows the eigenspectrum approaching the real axis as $I_e^1$ increases. Results are for $\sigma_e = \sigma_i = 6.25$ and $K_{glob} = 0.2$.

https://doi.org/10.1371/journal.pcsy.0000057.g008

($K_{glob} < 0$). However, with increasing $K_{glob}$, higher levels of heterogeneity within the neuronal populations become necessary to trivialize the system effectively.

We then investigated how differential heterogeneity in E and I sub-populations affects the trivialization process. In Fig 11, we show how the manifolds change within $(\sigma_e, \sigma_i)$ space as $K_{glob}$ changes. Irrespective of the coupling strength, the two-node network shows regions with multiple equilibria until $\sigma_i \simeq 10$ for homogeneous E sub-populations. In Fig 11a, we observe that with an excitatory heterogeneity of $\sigma_e > 5$, the system can be trivialized in the presence of homogeneous I sub-populations. However, as $K_{glob}$ increases, the required amount of excitatory heterogeneity to quench multi-stability increases as shown in Fig 11b–11d. Notably, when $K_{glob} = 0.8$, the trivialization is predominantly led by the inhibitory heterogeneity with $\sigma_i > 10$.

To investigate the increase in excitatory heterogeneity with $K_{glob}$, we analyzed the equilibria for the system configuration at points **A1** and **D1** in Fig 11. The results are shown in Fig 12. For $K_{glob} = -0.8$, the system is trivialized and exhibits higher resilience to external stimulations, with $\zeta < 0$ as seen in Fig 12a. In this case, the system remains in a stable spiral state for all modulatory inputs. However, for $K_{glob} = 0.8$ (Fig 12b), we observe multi-stability even with increased heterogeneity in the E sub-populations. The network transitions from

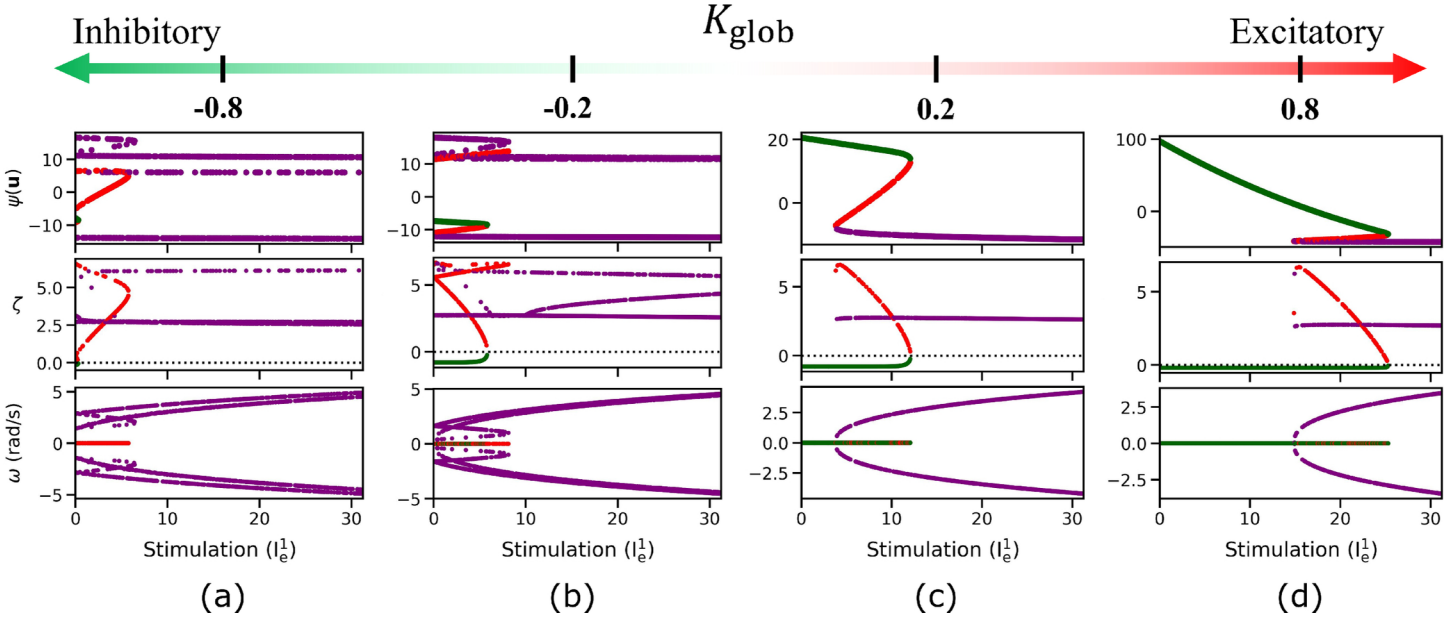


**Fig 9. Global coupling parameter's effect on trivializing the two-node system is less significant compared to heterogeneity.** Sub-figures labeled (a) to (d) depict four different $K_{glob}$ values. Each sub-figure has three panels: (i) the dimension-reduced equilibria, with colors representing different stable states as defined (Table 2), (ii) maximum damping ratio $\zeta$, and (iii) significant oscillatory rates $\omega$. Results are for $\sigma = 2.5$ with $\mathcal{C}$–A i.e., $\sigma_e = \sigma_i = \sigma$.

https://doi.org/10.1371/journal.pcsy.0000057.g009

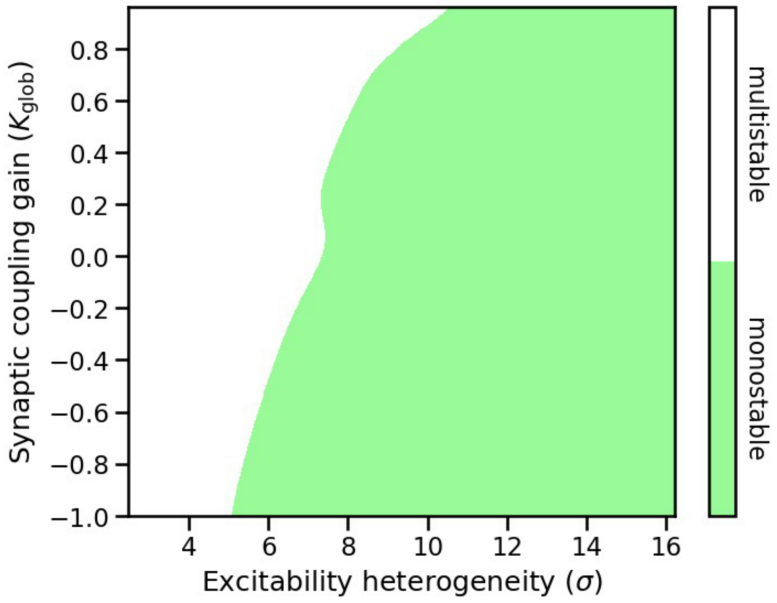


**Fig 10. As coupling strength increases, the network demands higher excitability heterogeneity for system trivialization.** The binarized map indicates the presence of multiple equilibria for a network with a specific $(K_{glob}, \sigma)$ pair as $I_e^1$ varies. A pixel value of 1 is assigned if $\Delta I_e^1 > 0$, indicating the presence of multiple equilibria; otherwise, it is set to 0. The results are derived using $\mathcal{C}$–A, where $\sigma_e = \sigma_i = \sigma$.

https://doi.org/10.1371/journal.pcsy.0000057.g010

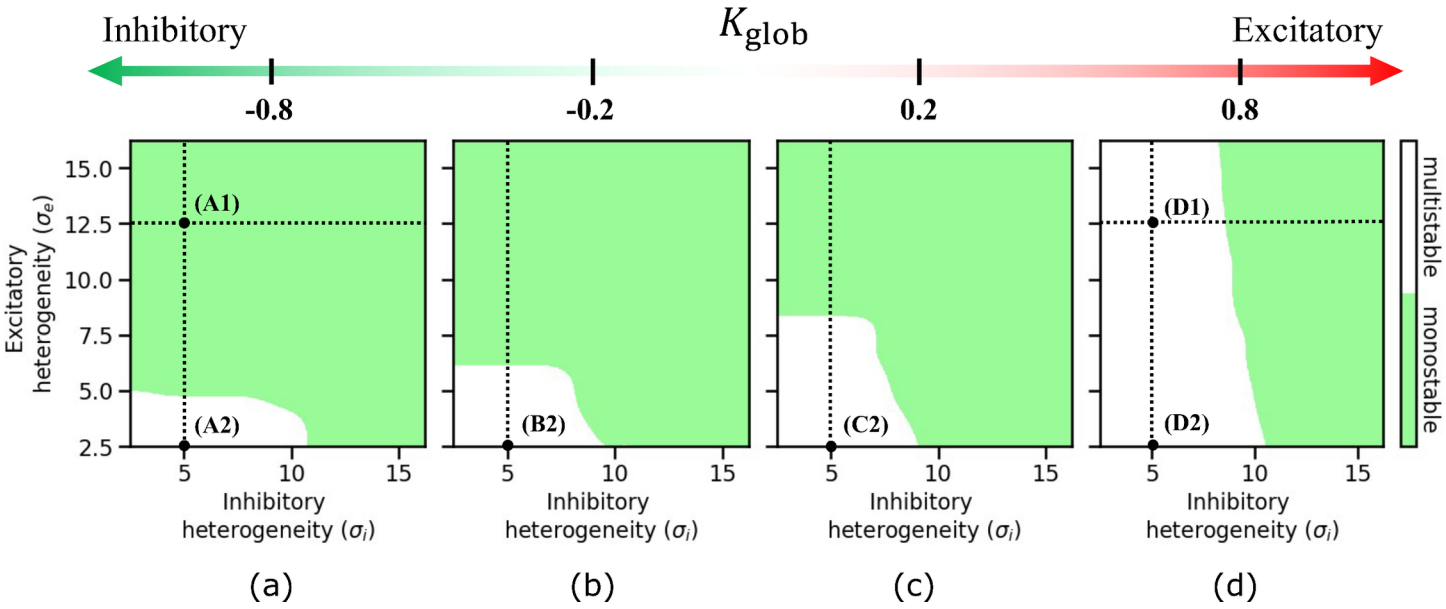


**Fig 11. As $K_{glob}$ increases, the effectiveness of excitatory heterogeneity in trivializing the system diminishes, with inhibitory heterogeneity emerging as the most significant property for trivialization.** The sub-figures (a) – (d) are binarized maps indicating the presence of multiple equilibria for a network with a specific $(\sigma_e, \sigma_i)$ pair for a given $K_{glob}$ as $I_e^1$ varies. In each sub-figure, a pixel value of 1 is assigned if $\Delta I_e^1 > 0$, indicating the presence of multiple equilibria; otherwise, it is set to 0. The results are derived using $\mathcal{C}$–B i.e., independently changing $\sigma_e$ and $\sigma_i$.

https://doi.org/10.1371/journal.pcsy.0000057.g011

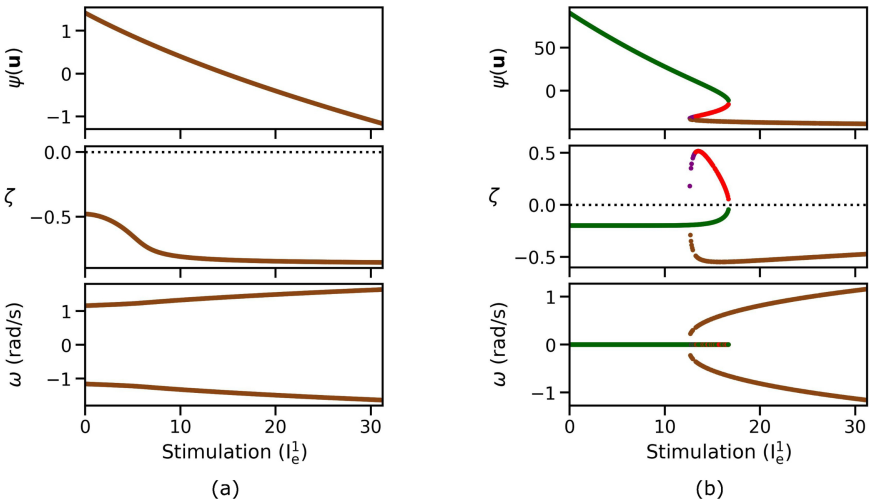


**Fig 12. Increase in $K_{glob}$ reveals multi-stable vicinities in the dynamic field of the network.** The sub-figures (a) and (b) are associated with points **A1** and **D1** in Fig 11 respectively.

https://doi.org/10.1371/journal.pcsy.0000057.g012

a stable node to a stable spiral, as shown in Fig 13, after crossing the multi-stable region. The positive feedback between nodes shifts the network dynamics into a higher stimulation regime, revealing multi-stable regions that appear with negative stimulation when $K_{glob} <$ 0. The network remains as a spiral sink at higher stimulations, as shown in Fig 13b, in contrast to the behavior observed in Fig 8b. This difference arises because the eigenvalues of the

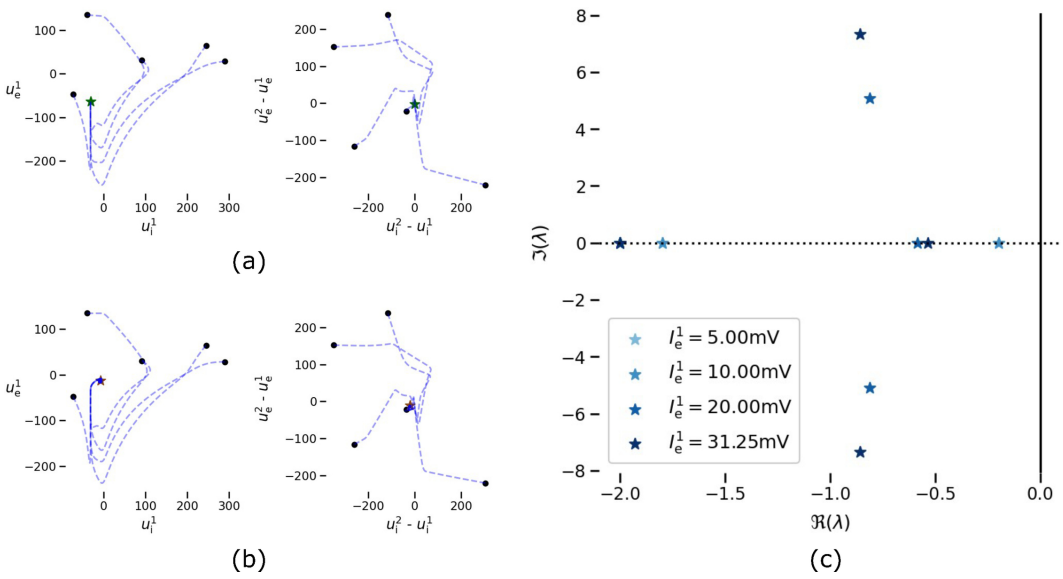


**Fig 13. Macro-scale dynamics at different $I_e^1$ in Fig 12b.** Sub-figures (a) and (b) show 2D phase portrait on node 1 and cross-node planes for $I_e^1 = 5$ mV and $I_e^1 = 31.25$ mV, respectively. Sub-figure (c) shows that the eigenspectrum resides well inside of the left half-plane. Results are for $\sigma_e = 12$, $\sigma_i = 5$ and $K_{glob} = 0.8$.

https://doi.org/10.1371/journal.pcsy.0000057.g013

equilibria at higher stimulation for the system corresponding to Fig 12b lie firmly within the left half-plane of the complex plane, as illustrated in Fig 8c.

We further observe the shift in the dynamic field and the emergence of multi-stable regions as $K_{glob}$ changes, as shown in Fig 14. By comparing Fig 12 with Fig 14, we note that higher excitatory heterogeneity improves resilience against stronger stimulation, even as the dynamic field is translated by $K_{glob}$. Particularly, in Fig 12a, the system exhibits stable spirals (brown

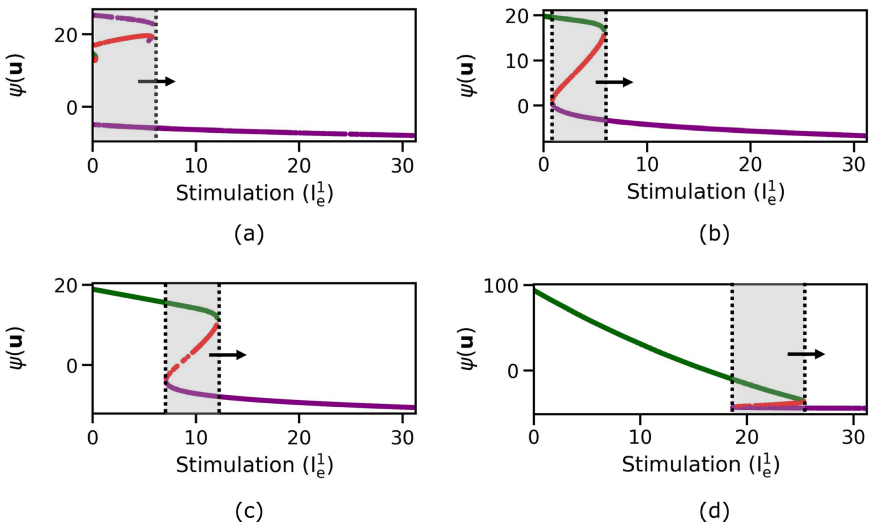


**Fig 14. An increase in $K_{glob}$ shifts the multi-stable regions towards stronger stimulations, enhancing stability against weaker stimulations.** Sub-figures (a)–(d) corresponds to **(A2)**–**(D2)** in Fig 11.

https://doi.org/10.1371/journal.pcsy.0000057.g014

points) compared to unstable spirals (purple points) in Fig 14a for higher stimulation. Furthermore, comparing Fig 12b to 14d, we note that the system with a higher excitatory heterogeneity achieves resilience against stronger stimulation compared to a lower excitatory heterogeneity of $\sigma_e = 2.5$. These results highlight the significance of both inhibitory and excitatory heterogeneities in maintaining resilience against external stimulation. However, when multi-stable regions appear as a result of a shift in the dynamic field when coupling changes, excitatory heterogeneity alone may not effectively quench the multiple equilibria present at some $I_e^1$. However, sufficiently high heterogeneous I sub-populations can consistently render macro-scale networks both resilient and trivialized.

## 4. Extending analysis with a multi-node (*N*>2) macro-scale brain network

This section examines the generalizability of the claims from Sect 3 using a multi-node macro-scale network with $N = 90$ nodes. The setup mirrors the two-node system, with $\mathbf{P} = [\, p_{nm} \,] \in \mathbb{R}^{90\times 90}$ representing pairwise structural associations. We use structural connectivity in [66] that are based on DTI and AAL brain atlas [67]. To simplify the simulation setup, we assign the same heterogeneity parameters across all nodes, but differentially to excitatory and inhibitory sub-populations. Stimulation is applied to the node with the highest degree, with results averaged over 10 trials. In each trial, the structural connectivity data from one randomly selected patient out of 88 creates the macro-scale brain network, ensuring consistency across labeled anatomical regions. Network behavior is analyzed for $K_{\text{glob}} \in [-1, 1)$, and Fig 15 summarizes the network setup and degree distribution for each node $n \in [90]$, defined as $\mathrm{D}^n = \sum_{m=1}^{N} p_{nm}$.

Fig 16 illustrates the Lyapunov stability of the modulated node within a multi-node macro-scale brain network. Similar to Sect 3.2, we observe a differential effect on Lyapunov stability between excitatory and inhibitory heterogeneity.

We observe that the network achieves stability with lower global coupling when sufficient inhibitory heterogeneity is present (green and purple curves), compared to networks with homogeneous I sub-populations (red and purple curves). Stability improves further when both sub-populations are heterogeneous, allowing the network to remain stable across the entire range of $K_{\text{glob}}$ considered. These results are consistent with the parameter manifolds

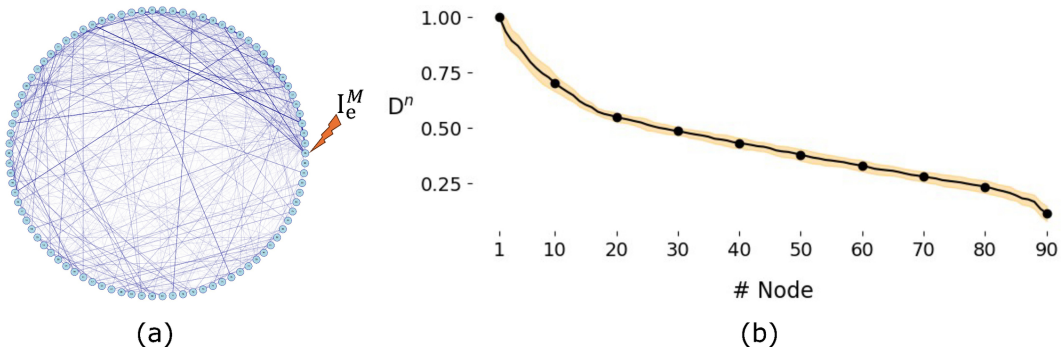


**Fig 15. Multi-node macro-scale network and the degree distributions of each node.** Sub-figure (a) shows the multi-node structural network with average connectivity across 10 realizations of **P**. Sub-figure (b) displays the degrees of each node $n \in [90]$, denoted by $\mathrm{D}^n$, with the black curve representing the average degree and error bars indicating the spread across trials.

https://doi.org/10.1371/journal.pcsy.0000057.g015

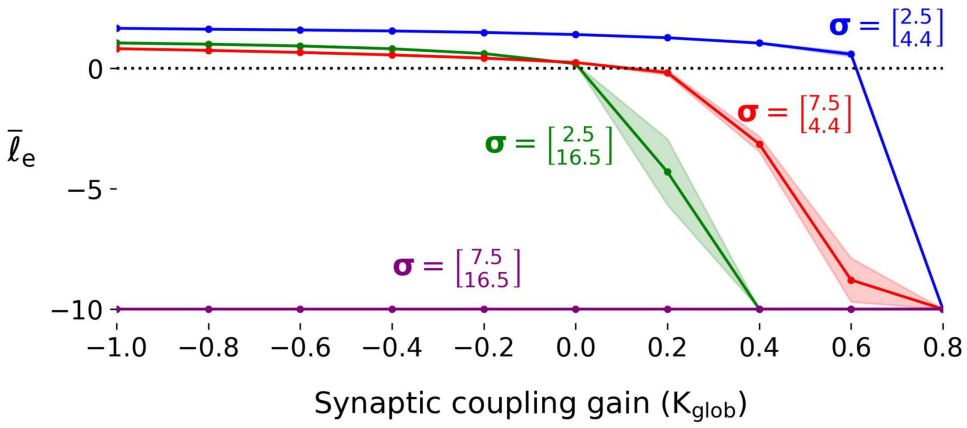


**Fig 16. Multi-node macro-scale networks show Lyapunov stability with excitability heterogeneity similar to that observed in two-node networks.** The figure shows a similar impact of excitatory heterogeneity, which is contingent upon the inhibitory heterogeneity present in the network. Node 1 is stimulated with $I_e^M = 31.25$ mV.

https://doi.org/10.1371/journal.pcsy.0000057.g016

presented in Sect 3.2. Similar to the two-node network, highly unstable dynamics emerge in the stimulated brain region as global coupling becomes inhibitory. Specifically, with lower excitatory heterogeneity, increasing inhibitory heterogeneity (green curve) leads to greater Lyapunov instability compared to networks with heterogeneous E sub-populations and homogeneous inhibitory I sub-populations (red curve). Thus, the findings from the two-node network regarding stability with excitability heterogeneity and global synaptic coupling can be generalized to larger multi-node macro-scale networks, offering a broader representation of the human brain at the macro-scale.

Fig 17 shows that multi-node macro-scale brain networks become trivialized with higher excitability heterogeneity for a given $K_{glob}$. Row R1 in Fig 17 illustrates that multi-stable regions appear in networks with homogeneous sub-populations across all $K_{glob}$, making them less resilient to stronger stimulation. As $K_{glob}$ becomes excitatory, the dynamic field shifts, leading to stable node states (green-colored equilibria states) for a broader range of external stimulation and confining instability to stronger stimulation. Higher inhibitory heterogeneity trivializes the network, as seen in rows R2 and R3 in Fig 17. Though less significant than inhibitory heterogeneity in trivializing the network, excitatory heterogeneity enhances resilience, especially when $K_{glob} < 0$, as shown in columns (a) and (b) of rows R2 and R3 in Fig 17. Networks with increased excitatory heterogeneity exhibit stable spirals over the entire modulatory range, contrasting with the unstable spirals in homogeneous E sub-populations. This suggests that the network undergoes an Adronov-Hopf bifurcation as the excitatory heterogeneity increases at least for the inhibitory coupling and stronger stimulation, as shown in columns (a) and (b) of rows R2 and R3 in Fig 17.

These results mirror those in Sect 3.3. Overall, increased heterogeneity in neuronal populations improves resilience against external stimulations. However, excitatory heterogeneity is less effective than inhibitory heterogeneity at reducing multiple equilibria. Increasing $K_{glob}$ shifts the dynamic fields and enhances resilience, especially towards a stable node state. Thus, the multi-node network confirms that excitability heterogeneity and global synaptic coupling strength are crucial for maintaining brain stability and resilience, highlighting the importance of inhibitory heterogeneity.

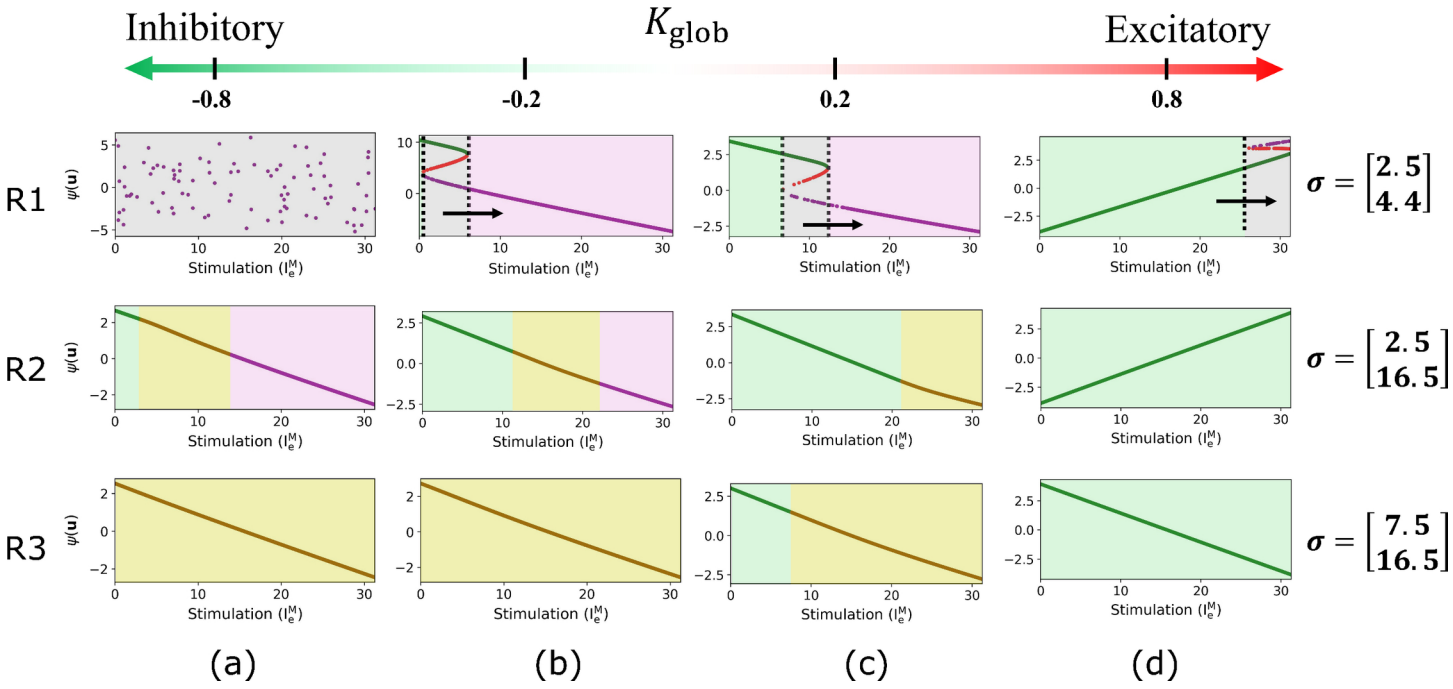


**Fig 17. Multi-node macro-scale networks show trivialization with excitability heterogeneity similar to that observed in two-node networks.** Each sub-figure, organized in a 3×4 grid, shows the progression of equilibria with $I_e^M$ for specific heterogeneity vectors $\boldsymbol{\sigma}$ and global coupling strengths $K_{glob}$. Colors indicate stable states at each equilibrium, as defined in Table 2. Rows R1 to R3 represent different heterogeneity vectors. Columns (a) to (d) correspond to different values of $K_{glob}$.

https://doi.org/10.1371/journal.pcsy.0000057.g017

## 5. Discussion

This study explores the role of excitability heterogeneity in networked macro-scale brain dynamics, focusing on how neuronal diversity, particularly the dispersion of firing thresholds, influences network stability and trivialization. By explicitly modeling excitability heterogeneity, we demonstrate its significant impact on stability and resilience in large-scale brain networks.

The role of excitability heterogeneity in providing intrinsic homeostatic control against external perturbations has been established both analytically and numerically [16,56]. Such control has shown prominent protection against epileptogenesis within the human brain [6,14,16,44]. Previous studies have explored how excitatory and inhibitory neuronal heterogeneity affect stability, synchronization, and firing activities [14,20], and its influence on neural coding and computations, including learning in spiking neural networks [12,15]. However, these studies largely focus on microcircuits where individual neurons are network nodes, limiting their clinical relevance due to difficulties in sensing individual neural activity.

Other works have examined the stability and synchronization of fractional-order systems applied to neural networks, focusing on equilibrium points, stabilization, and bifurcation dynamics [68–73]. Simplified neocortical models, such as two-node Hopfield networks, have highlighted the emergence of multi-stability and bifurcation regions by varying excitatory and inhibitory connectivity [74]. However, these analyses often overlook how neuronal heterogeneity impacts network stability. In contrast, we explicitly model the variability in excitability and show its pivotal role in maintaining stability and resilience, particularly with global synaptic coupling. Additionally, we highlight how excitability heterogeneity trivializes

macro-scale dynamics by expanding the range of stable states under external stimulations, thus avoiding bifurcations.

In line with prior work, [17,75], which emphasizes the stabilizing effects of neuronal diversity in preventing multi-stable states, our findings confirm that excitability heterogeneity is essential for network resilience at the macro-scale. Specifically, we show that the interplay between neuronal heterogeneity and inter-regional coupling critically influences network stability as external stimulations act upon its nodes. Similarly, [56] observed that noise as a stimulation suppresses multi-stability by aligning system responses with input magnitude. Our work extends these findings by examining how excitability heterogeneity and global synaptic coupling influence multi-region networks, offering insights into macro-scale brain dynamics.

Studies on whole-brain models have shown that regional heterogeneity in excitation-inhibition ratios impacts large-scale dynamics, such as information transmission and resting-state connectivity [29,37,43]. While these models emphasize regional diversity for empirical fidelity, they often neglect how heterogeneity levels affect dynamic properties. We address this gap by analyzing the effects of excitability heterogeneity across a broad spectrum, providing a nuanced understanding of its role in stabilizing macro-scale networks.

Our results demonstrate that excitability heterogeneity enhances network stability. For both excitatory and inhibitory sub-populations, increased heterogeneity bolsters resilience to external stimulations, aligning with previous findings [16,17,56] except at the macro-scale. We observe a differential impact: inhibitory heterogeneity ($\sigma_i$) is more effective at reducing multi-stable regions and enhancing stability across a range of global coupling strengths ($K_{glob}$), particularly in multi-node networks. High inhibitory heterogeneity consistently stabilizes the system, even under varying stimulations. Excitatory heterogeneity ($\sigma_e$) has a more conditional role. It enhances stability in the presence of inhibitory heterogeneity but increases instability when inhibitory populations are highly homogeneous. Beyond a certain threshold, however, excitatory heterogeneity eliminates this instability. While less effective at reducing multiple equilibria, it significantly mitigates the impact of external stimulation, particularly in networks with inhibitory global coupling ($K_{glob} < 0$).

Synaptic coupling between brain regions plays a crucial role in network dynamics. We identify a synergistic effect between excitability heterogeneity and global synaptic coupling in achieving Lyapunov stability. As $K_{glob}$ becomes more excitatory, the dynamic field shifts, stabilizing node states across a broader range of stimulations and confining instability to stronger stimulations. However, the trivializing effect of excitatory heterogeneity diminishes with increasing $K_{glob}$, highlighting the dominant role of inhibitory heterogeneity in stabilizing the system.

In summary, our study highlights the crucial role of excitability heterogeneity in shaping macro-scale brain dynamics, providing insights into the interplay between neuronal diversity and synaptic coupling in maintaining stability and resilience. Although methods such as Floquet theory [76,77] and their computational implementations offer a promising way to study how excitability heterogeneity shapes non-equilibrium (i.e., periodic) dynamics in high-dimensional brain networks, such an analysis is beyond the scope of the present work. This offers a promising direction for future work, such as designing control strategies to reach desired states.

## 5.1. Limitations and future work

While our study demonstrates the generalizability of the claims with a larger macro-scale brain network, several limitations remain. Firstly, it remains open to debate whether the

heterogeneity of the firing thresholds of the neurons is an appropriate representation of the intrinsic heterogeneity of the neurons within the human brain. Secondly, our model assumes uniform neuronal heterogeneity across all brain regions. In reality, each region may exhibit distinct neuronal diversity, which can potentially alter macro-scale dynamics. Future work should incorporate region-specific heterogeneity for a more accurate representation. Third, our model lacks empirical validation using in vivo data on excitability heterogeneity from different brain regions and electrophysiological activities. This gap highlights the need to bridge the mathematical analysis with biophysical reality, particularly with regard to how excitability heterogeneity affects Lyapunov stability and resilience. Such validation could provide biophysically plausible intrinsic heterogeneity levels within each brain region to better represent and interpret actual brain states. Another important limitation is the omission of transmission delays between brain regions. Although delays greatly affect synchronization and dynamics, including them would increase model complexity significantly. To analyze the effect of excitability heterogeneity on macro-scale brain networks, we limited this study to delay-free networks. Future work will incorporate delays to provide a more complete understanding of their impact. Lastly, extending our analysis to different network topologies is crucial for validating findings in more complex brain models. Future research should also consider implications for pathological brain states, such as epilepsy and neurodegenerative diseases, and explore potential therapeutic interventions. Addressing these limitations will lead to a more comprehensive understanding of brain network dynamics and their role in stability and resilience.

## 6. Conclusion

In summary, our research emphasizes the critical role of neural diversity, particularly excitability heterogeneity, in understanding the complexities of brain dynamics and its modulation at a broader spatial scale. By analyzing macro-scale dynamics using a two-region model, we've highlighted how balanced excitatory and inhibitory heterogeneity, along with synaptic coupling, are essential for maintaining stability within neural networks. Our findings reveal the adverse effects of excessive excitatory heterogeneity, especially noticeable at weaker stimulations, underscoring the delicate balance required for neural stability. Furthermore, our exploration through linear stability analysis uncovers the presence of multi-stable transitions, which are mitigated by excitability diversity. Extending our analysis to a multi-node macro-scale network, we've demonstrated the generalizability of results from a two-node network to a more complex architecture of whole-brain modeling using neuroimaging data. By shedding light on these phenomena, our research not only advances our understanding of brain function but also emphasizes the intricate interplay of neural diversity in shaping neural network behavior at a broader spatial scale. This insight lays the foundation for future investigations aimed at unraveling the complexities of neural systems and their modulation from a whole-brain perspective.

## Supporting information

**S1 Appendix. Linearization of the system around equilibria using Jacobian Matrix.** This section highlights how the linearization of the macro-scale brain network is carried out using the Jacobian matrix and evaluates the system behavior.
(PDF)

**S2 Appendix. Dimensional reduction to visualize equilibrium points and system behavior using linear stability analysis.**
(PDF)

**S3 Appendix. State transition boundary does not change with additive Gaussian Noise within $(K_{glob}, \sigma)$ parameter space.** The impact of environmental noise on the stability of macro-scale dynamics was investigated using $\mathcal{C}$–A.
(PDF)

**S4 Appendix. State transition boundary change as modulatory signal changes within $(\sigma_e, \sigma_i)$ parameter space for given $K_{glob}$.** This section provides supplementary materials from Sect 3.2, illustrating the transition boundaries within the $(\sigma_e, \sigma_i)$ parameter space for different $I_e^1$.
(PDF)

**S5 Appendix. Investigation of numerical stability as integration step size $\Delta t$ changes.** This section illustrates results for Lyapunov stability analysis with different integral step sizes. The results are obtained with the two-node system illustrating the transition boundaries within the $(K_{glob}, \sigma)$ parameter space for different $\Delta t$.
(PDF)

**S6 Appendix. Two-Parameter Bifurcation Analysis of the Single-Node Brain Model** This section illustrates the two-parameter bifurcation results for the single-node brain model defined in Eq (1). The analysis is further extended to obtain preliminary two-parameter bifurcation results for the coupled two-node macro-scale brain model.
(PDF)

## Author contributions

**Conceptualization:** Kalana G. Abeywardena, Jeremie Lefebvre, Taufik A. Valiante, Stark C. Draper.

**Formal analysis:** Kalana G. Abeywardena.

**Funding acquisition:** Stark C. Draper.

**Investigation:** Kalana G. Abeywardena.

**Methodology:** Kalana G. Abeywardena.

**Project administration:** Stark C. Draper.

**Resources:** Jeremie Lefebvre, Taufik A. Valiante, Stark C. Draper.

**Software:** Kalana G. Abeywardena.

**Supervision:** Stark C. Draper.

**Visualization:** Kalana G. Abeywardena.

**Writing – original draft:** Kalana G. Abeywardena.

**Writing – review & editing:** Kalana G. Abeywardena, Jeremie Lefebvre, Taufik A. Valiante, Stark C. Draper.

## References


1. Eberwine J, Kim J. Cellular deconstruction: finding meaning in individual cell variation. Trends Cell Biol. 2015;25(10):569–78. https://doi.org/10.1016/j.tcb.2015.07.004 PMID: 26410403
2. Dueck H, Eberwine J, Kim J. Variation is function: are single cell differences functionally important?: Testing the hypothesis that single cell variation is required for aggregate function. Bioessays. 2016;38(2):172–80. https://doi.org/10.1002/bies.201500124 PMID: 26625861
3. Zeng H. What is a cell type and how to define it?. Cell. 2022;185(15):2739–55. https://doi.org/10.1016/j.cell.2022.06.031 PMID: 35868277
4. Cembrowski MS, Menon V. Continuous variation within cell types of the nervous system. Trends Neurosci. 2018;41(6):337–48.
5. Cembrowski MS, Spruston N. Heterogeneity within classical cell types is the rule: lessons from hippocampal pyramidal neurons. Nat Rev Neurosci. 2019;20(4):193–204. https://doi.org/10.1038/s41583-019-0125-5 PMID: 30778192
6. Moradi Chameh H, Rich S, Wang L, Chen F-D, Zhang L, Carlen PL, et al. Diversity amongst human cortical pyramidal neurons revealed via their sag currents and frequency preferences. Nat Commun. 2021;12(1):2497. https://doi.org/10.1038/s41467-021-22741-9 PMID: 33941783
7. Padmanabhan K, Urban NN. Intrinsic biophysical diversity decorrelates neuronal firing while increasing information content. Nat Neurosci. 2010;13(10):1276–82. https://doi.org/10.1038/nn.2630 PMID: 20802489
8. Tripathy SJ, Padmanabhan K, Gerkin RC, Urban NN. Intermediate intrinsic diversity enhances neural population coding. Proc Natl Acad Sci U S A. 2013;110(20):8248–53. https://doi.org/10.1073/pnas.1221214110 PMID: 23630284
9. Brette R. Computing with neural synchrony. PLoS Comput Biol. 2012;8(6):e1002561. https://doi.org/10.1371/journal.pcbi.1002561 PMID: 22719243
10. Shamir M, Sompolinsky H. Implications of neuronal diversity on population coding. Neural Comput. 2006;18(8):1951–86. https://doi.org/10.1162/neco.2006.18.8.1951 PMID: 16771659
11. Chelaru MI, Dragoi V. Efficient coding in heterogeneous neuronal populations. Proc Natl Acad Sci. 2008;105(42):16344–9.
12. Perez-Nieves N, Leung VCH, Dragotti PL, Goodman DFM. Neural heterogeneity promotes robust learning. Nat Commun. 2021;12(1):5791. https://doi.org/10.1038/s41467-021-26022-3 PMID: 34608134
13. Mejias JF, Longtin A. Optimal heterogeneity for coding in spiking neural networks. Phys Rev Lett. 2012;108(22):228102. https://doi.org/10.1103/PhysRevLett.108.228102 PMID: 23003656
14. Rich S, Moradi Chameh H, Lefebvre J, Valiante TA. Loss of neuronal heterogeneity in epileptogenic human tissue impairs network resilience to sudden changes in synchrony. Cell Rep. 2022;39(8):110863. https://doi.org/10.1016/j.celrep.2022.110863 PMID: 35613586
15. Gast R, Solla SA, Kennedy A. Neural heterogeneity controls computations in spiking neural networks. Proc Natl Acad Sci U S A. 2024;121(3):e2311885121. https://doi.org/10.1073/pnas.2311885121 PMID: 38198531
16. Hutt A, Rich S, Valiante TA, Lefebvre J. Intrinsic neural diversity quenches the dynamic volatility of neural networks. Proc Natl Acad Sci. 2023;120(28):e2218841120.
17. Hutt A, Trotter D, Pariz A, Valiante TA, Lefebvre J. Diversity-induced trivialization and resilience of neural dynamics. Chaos: An Interdiscip J Nonl Sci. 2024;34(1).
18. Hass J, Hertäg L, Durstewitz D. A detailed data-driven network model of prefrontal cortex reproduces key features of in vivo activity. PLoS Comput Biol. 2016;12(5):e1004930. https://doi.org/10.1371/journal.pcbi.1004930 PMID: 27203563
19. Hass J, Ardid S, Sherfey J, Kopell N. Constraints on persistent activity in a biologically detailed network model of the prefrontal cortex with heterogeneities. Prog Neurobiol. 2022;215:102287. https://doi.org/10.1016/j.pneurobio.2022.102287 PMID: 35533813
20. Mejias JF, Longtin A. Differential effects of excitatory and inhibitory heterogeneity on the gain and asynchronous state of sparse cortical networks. Front Comput Neurosci. 2014;8:107. https://doi.org/10.3389/fncom.2014.00107 PMID: 25309409
21. Quarta C, Claret M, Zeltser LM, Williams KW, Yeo GS, Tschöp MH. POMC neuronal heterogeneity in energy balance and beyond: an integrated view. Nature Metabolism. 2021;3(3):299–308.
22. Duarte R, Morrison A. Leveraging heterogeneity for neural computation with fading memory in layer 2/3 cortical microcircuits. PLoS Comput Biol. 2019;15(4):e1006781. https://doi.org/10.1371/journal.pcbi.1006781 PMID: 31022182
23. Bui A, Kim HK, Maroso M, Soltesz I. Microcircuits in epilepsy: heterogeneity and hub cells in network synchronization. Cold Spring Harb Perspect Med. 2015;5(11):a022855. https://doi.org/10.1101/cshperspect.a022855 PMID: 26525454

24. Buzsáki G, Anastassiou CA, Koch C. The origin of extracellular fields and currents–EEG, ECoG, LFP and spikes. Nat Rev Neurosci. 2012;13(6):407–20. https://doi.org/10.1038/nrn3241 PMID: 22595786
25. Nunez PL, Srinivasan R. Electric fields of the brain: the neurophysics of EEG. USA: Oxford University Press; 2006.
26. Wilson HR, Cowan JD. Excitatory and inhibitory interactions in localized populations of model neurons. Biophys J. 1972;12(1):1–24. https://doi.org/10.1016/S0006-3495(72)86068-5 PMID: 4332108
27. Pathak A, Roy D, Banerjee A. Whole-brain network models: from physics to bedside. Front Comput Neurosci. 2022;16:866517. https://doi.org/10.3389/fncom.2022.866517 PMID: 35694610
28. Gerstner W, Kistler WM, Naud R, Paninski L. Neuronal dynamics: from single neurons to networks and models of cognition. Cambridge University Press; 2014.
29. Deco G, Ponce-Alvarez A, Hagmann P, Romani GL, Mantini D, Corbetta M. How local excitation–inhibition ratio impacts the whole brain dynamics. J Neurosci. 2014;34(23):7886–98.
30. Garey LJ. Brodmann's localisation in the cerebral cortex. World Scientific; 1999.
31. Dayan P, Abbott LF. Theoretical neuroscience: computational and mathematical modeling of neural systems. J Cognit Neurosci. 2003;15(1):154–5.
32. Hagmann P, Cammoun L, Gigandet X, Meuli R, Honey CJ, Wedeen VJ, et al. Mapping the structural core of human cerebral cortex. PLoS Biol. 2008;6(7):e159. https://doi.org/10.1371/journal.pbio.0060159 PMID: 18597554
33. Negi SK, Guda C. Global gene expression profiling of healthy human brain and its application in studying neurological disorders. Sci Rep. 2017;7(1):897. https://doi.org/10.1038/s41598-017-00952-9 PMID: 28420888
34. Fornito A, Arnatkevičiūtė A, Fulcher BD. Bridging the gap between connectome and transcriptome. Trends Cogn Sci. 2019;23(1):34–50. https://doi.org/10.1016/j.tics.2018.10.005 PMID: 30455082
35. Buch AM, Vértes PE, Seidlitz J, Kim SH, Grosenick L, Liston C. Molecular and network-level mechanisms explaining individual differences in autism spectrum disorder. Nat Neurosci. 2023;26(4):650–63. https://doi.org/10.1038/s41593-023-01259-x PMID: 36894656
36. Deco G, Kringelbach ML, Arnatkeviciute A, Oldham S, Sabaroedin K, Rogasch NC. Sci Adv. 2021;7(29):eabf4752. https://doi.org/10.1126/sciadv.abf4752
37. Demirtaş M, Burt JB, Helmer M, Ji JL, Adkinson BD, Glasser MF, et al. Hierarchical heterogeneity across human cortex shapes large-scale neural dynamics. Neuron. 2019;101(6):1181-1194.e13. https://doi.org/10.1016/j.neuron.2019.01.017 PMID: 30744986
38. Suárez LE, Markello RD, Betzel RF, Misic B. Linking structure and function in macroscale brain networks. Trends Cogn Sci. 2020;24(4):302–15. https://doi.org/10.1016/j.tics.2020.01.008 PMID: 32160567
39. Atasoy S, Donnelly I, Pearson J. Human brain networks function in connectome-specific harmonic waves. Nat Commun. 2016;7:10340. https://doi.org/10.1038/ncomms10340 PMID: 26792267
40. Pang JC, Aquino KM, Oldehinkel M, Robinson PA, Fulcher BD, Breakspear M, et al. Geometric constraints on human brain function. Nature. 2023;618(7965):566–74. https://doi.org/10.1038/s41586-023-06098-1 PMID: 37258669
41. Perl YS, Zamora-Lopez G, Montbrió E, Monge-Asensio M, Vohryzek J, Fittipaldi S, et al. The impact of regional heterogeneity in whole-brain dynamics in the presence of oscillations. Netw Neurosci. 2023;7(2):632–60. https://doi.org/10.1162/netn_a_00299 PMID: 37397876
42. Huntenburg JM, Bazin P-L, Margulies DS. Large-scale gradients in human cortical organization. Trends Cogn Sci. 2018;22(1):21–31. https://doi.org/10.1016/j.tics.2017.11.002 PMID: 29203085
43. Deco G, Cabral J, Woolrich MW, Stevner ABA, van Hartevelt TJ, Kringelbach ML. Single or multiple frequency generators in on-going brain activity: a mechanistic whole-brain model of empirical MEG data. Neuroimage. 2017;152:538–50. https://doi.org/10.1016/j.neuroimage.2017.03.023 PMID: 28315461
44. Chameh HM, Falby M, Movahed M, Arbabi K, Rich S, Zhang L, et al. Distinctive biophysical features of human cell-types: insights from studies of neurosurgically resected brain tissue. Front Synaptic Neurosci. 2023;15:1250834. https://doi.org/10.3389/fnsyn.2023.1250834 PMID: 37860223
45. Si A m a r i. Field theory of self-organizing neural nets. IEEE Trans Syst Man Cybernet. 1983;(5):741–8.
46. Lynn CW, Bassett DS. The physics of brain network structure, function, and control. Nat Rev Phys. 2019;1(5):318–32.
47. Gluss B. A model for neuron firing with exponential decay of potential resulting in diffusion equations for probability density. Bull Math Biophys. 1967;29(2):233–43. https://doi.org/10.1007/BF02476897 PMID: 4293111

48. Herrmann CS, Murray MM, Ionta S, Hutt A, Lefebvre J. Shaping intrinsic neural oscillations with periodic stimulation. J Neurosci. 2016;36(19):5328–37. https://doi.org/10.1523/JNEUROSCI.0236-16.2016 PMID: 27170129
49. Lefebvre J, Hutt A, Frohlich F. Stochastic resonance mediates the state-dependent effect of periodic stimulation on cortical alpha oscillations. Elife. 2017;6:e32054. https://doi.org/10.7554/eLife.32054 PMID: 29280733
50. Lefebvre J, Hutt A. Induced synchronization by endogenous noise modulation in finite-size random neural networks: a stochastic mean-field study. Chaos: Interdiscip J Nonl Sci. 2023;33(12).
51. Ponce-Alvarez A, He BJ, Hagmann P, Deco G. Task-driven activity reduces the cortical activity space of the brain: experiment and whole-brain modeling. PLoS Comput Biol. 2015;11(8):e1004445. https://doi.org/10.1371/journal.pcbi.1004445 PMID: 26317432
52. El Houssaini K, Bernard C, Jirsa VK. The epileptor model: a systematic mathematical analysis linked to the dynamics of seizures, refractory status epilepticus, and depolarization block. eNeuro. 2020;7(2):ENEURO.0485-18.2019. https://doi.org/10.1523/ENEURO.0485-18.2019 PMID: 32066612
53. Jadi MP, Sejnowski TJ. Cortical oscillations arise from contextual interactions that regulate sparse coding. Proc Natl Acad Sci U S A. 2014;111(18):6780–5. https://doi.org/10.1073/pnas.1405300111 PMID: 24742427
54. Jadi MP, Sejnowski TJ. Regulating cortical oscillations in an inhibition-stabilized network. Proc IEEE. 2014;102(5):830–42.
55. Neske GT, Patrick SL, Connors BW. Contributions of diverse excitatory and inhibitory neurons to recurrent network activity in cerebral cortex. J Neurosci. 2015;35(3):1089–105. https://doi.org/10.1523/JNEUROSCI.2279-14.2015 PMID: 25609625
56. Rich S, Hutt A, Skinner FK, Valiante TA, Lefebvre J. Neurostimulation stabilizes spiking neural networks by disrupting seizure-like oscillatory transitions. Sci Rep. 2020;10(1):15408. https://doi.org/10.1038/s41598-020-72335-6 PMID: 32958802
57. Strogatz SH. Nonlinear dynamics and chaos: with applications to physics, biology, chemistry, and engineering. CRC Press; 2018.
58. Alligood KT, Sauer TD, Yorke JA, Chillingworth D. Chaos: an introduction to dynamical systems. SIAM Rev. 1998;40(3):732.
59. Freitas C, Macau E, Pikovsky A. Partial synchronization in networks of non-linearly coupled oscillators: the deserter hubs model. Chaos: Interdiscip J Nonl Sci. 2015;25(4).
60. Powell MJ. A hybrid method for nonlinear equations. Numerical methods for nonlinear algebraic equations. 1970. p. 87–161.
61. Schölkopf B, Smola A, Müller KR. Nonlinear component analysis as a kernel eigenvalue problem. Neural Comput. 1998;10(5):1299–319.
62. Berg J, Sorensen SA, Ting JT, Miller JA, Chartrand T, Buchin A. Human cortical expansion involves diversification and specialization of supragranular intratelencephalic-projecting neurons. BioRxiv. 2020:2020–03.
63. Berg J, Sorensen SA, Ting JT, Miller JA, Chartrand T, Buchin A, et al. Human neocortical expansion involves glutamatergic neuron diversification. Nature. 2021;598(7879):151–8. https://doi.org/10.1038/s41586-021-03813-8 PMID: 34616067
64. Saggio ML, Crisp D, Scott JM, Karoly P, Kuhlmann L, Nakatani M, et al. A taxonomy of seizure dynamotypes. Elife. 2020;9:e55632. https://doi.org/10.7554/eLife.55632 PMID: 32691734
65. Guckenheimer J, Holmes P. Nonlinear oscillations, dynamical systems, and bifurcations of vector fields. Springer; 2013.
66. Škoch A, Rehák Bučková B, Mareš J, Tintěra J, Sanda P, Jajcay L, et al. Human brain structural connectivity matrices-ready for modelling. Sci Data. 2022;9(1):486. https://doi.org/10.1038/s41597-022-01596-9 PMID: 35945231
67. Ota K, Oishi N, Ito K, Fukuyama H, SEAD-J Study Group. A comparison of three brain atlases for MCI prediction. J Neurosci Methods. 2014;221:139–50. https://doi.org/10.1016/j.jneumeth.2013.10.003 PMID: 24140118
68. Ding Z, Zeng Z, Wang L. Robust finite-time stabilization of fractional-order neural networks with discontinuous and continuous activation functions under uncertainty. IEEE Trans Neural Netw Learn Syst. 2018;29(5):1477–90. https://doi.org/10.1109/TNNLS.2017.2675442 PMID: 28362594
69. Song C, Cao J. Dynamics in fractional-order neural networks. Neurocomputing. 2014;142:494–8.
70. Chen L, Chai Y, Wu R, Ma T, Zhai H. Dynamic analysis of a class of fractional-order neural networks with delay. Neurocomputing. 2013;111:190–4.
71. Kaslik E, Sivasundaram S. Nonlinear dynamics and chaos in fractional-order neural networks. Neural Netw. 2012;32:245–56. https://doi.org/10.1016/j.neunet.2012.02.030 PMID: 22386788

**72.** Xiao M, Zheng WX, Jiang G, Cao J. Undamped oscillations generated by hopf bifurcations in fractional-order recurrent neural networks with caputo derivative. IEEE Trans Neural Netw Learn Syst. 2015;26(12):3201–14. https://doi.org/10.1109/TNNLS.2015.2425734 PMID: 25993707

**73.** Kaslik E. Analysis of two-and three-dimensional fractional-order Hindmarsh-Rose type neuronal models. Fract Calculus Appl Anal. 2017;20(3):623–45.

**74.** Visser S, Meijer HG, van Putten MJ, van Gils SA. Analysis of stability and bifurcations of fixed points and periodic solutions of a lumped model of neocortex with two delays. J Math Neurosci. 2012;2(1):8. https://doi.org/10.1186/2190-8567-2-8 PMID: 22655859

**75.** Fyodorov YV, Le Doussal P. Topology trivialization and large deviations for the minimum in the simplest random optimization. J Statist Phys. 2014;154(1):466–90.

**76.** Barone S, Narcowich M, Narcowich F. Floquet theory and applications. Phys Rev A. 1977;15(3):1109.

**77.** Klausmeier CA. Floquet theory: a useful tool for understanding nonequilibrium dynamics. Theor Ecol. 2008;1:153–61.